STScI | SPACE TELESCOPE SCIENCE INSTITUTE

TECHNICAL REPORT

Title: Accuracy and Precision of Centroid Algorithms in the `photutils` Python package for NIRISS Point Spread Functions	Doc #: JWST-STScI-008116, SM-12 Date: February 3, 2022 Rev:
Authors: Paul Goudfrooij Phone: 410-338-4981	Release Date:

1 Abstract

We analyze the accuracy and precision of centroid measurements of stars in a set of simulated NIRISS images of the so-called JWST calibration field, which is calibrated in absolute and relative astrometry onto the Gaia reference frame to an RMS precision of 2.6 mas. We compare several centroid algorithms available in the `photutils` python package, and we analyze the dependencies on filter pivot wavelength, measurement box size, and center position within a pixel. Under the common assumption that the NIRISS PSFs created by the `WebbPSF` package represent the on-sky PSFs correctly across the field of view, we recommend use of the `centroid_2dg` algorithm for NIRISS imaging when astrometric precision is essential.

2 Introduction

The accuracy and precision of astrometric measurements of stars in imaging data are very important for several key measurements during JWST instrument commissioning. Good examples are the precise location of the various instruments in the focal plane, spatial offsets between images taken using different filters, and spatial offsets between direct images and zeroth-order grism spectra for wide-field slitless spectroscopy. Obtaining high precision of astrometric measurements is especially challenging for NIRISS, since its point spread functions (hereafter PSFs) are strongly undersampled by the detector for most imaging filters. Specifically, the NIRISS detector is critically sampled at $\lambda = 4.1$ μm while its imaging filters have pivot wavelengths ranging from 0.9 to 4.8 μm (e.g., Goudfrooij et al. 2021).

In this report, we analyze the accuracy and precision of centroid measurements using a variety of algorithms available in the `photutils` python package, which is an affiliate package of `Astropy` (Astropy Collaboration et al. 2013, 2018). After analyzing the dependencies on filter pivot wavelength, measurement box size, center position within a pixel, and the choice of PSF full width at half maximum (hereafter FWHM), we present our recommendations for use in analysis scripts for the relevant NIRISS commissioning programs.

3 Data

The data used for this analysis comprises a set of NIRISS images created by Tony Sohn using the Python simulation package `Mirage`, written by Bryan Hilbert et al. The data consist of simulated scenes of the NIRISS images that will be taken during commissioning programs 1086

and 1088. `Mirage` produces output images in a format that is as close as possible to real JWST data, using information in actual APT proposals and JWST pipeline reference files along with PSFs created using the WebbPSF package (Perrin et al. 2012, 2014), thus allowing these images to be used for analysis software development and testing. We use the full-frame NIRISS images associated with Observation 1 in APT Program 1086 and Observations 1 and 3 in APT program 1088, whose specifics are tabulated below in Table 1. The target field of these images is the so-called "JWST Calibration Field" in the Large Magellanic Cloud (LMC), which is characterized by a 5′x5′ HST-based star catalog within a 12′x12′ ground-based catalog, astrometrically calibrated in astrometry on the Gaia reference frame to an overall RMS precision of 2.6 mas, corresponding to 0.04 NIRISS pixel (see Sahlmann 2017, 2019). APT Program 1086 observed a field within the 5′x5′ HST catalog, while Program 1088 observed a field covered only by ground-based data.

Table 1: Properties of simulated images from APT programs 1086 and 1088 used for this analysis

FITS file root name	Filter	Pattern	NGROUPS	NINTS	Dither ID
jw01086001001_01101_00001_nis	F277W	NISRAPID	10	1	1
jw01086001001_01101_00003_nis	F444W	NISRAPID	10	1	1
jw01086001001_01101_00005_nis	F356W	NISRAPID	10	1	1
jw01086001001_01101_00007_nis	F430M	NISRAPID	15	1	1
jw01086001001_01101_00009_nis	F380M	NISRAPID	15	1	1
jw01086001001_01101_00011_nis	F480M	NISRAPID	15	1	1
jw01086001001_01101_00013_nis	F090W	NISRAPID	5	1	1
jw01086001001_01101_00015_nis	F115W	NISRAPID	5	1	1
jw01086001001_01101_00017_nis	F158M	NISRAPID	5	1	1
jw01086001001_01101_00019_nis	F140M	NISRAPID	5	1	1
jw01086001001_01101_00021_nis	F150W	NISRAPID	5	1	1
jw01086001001_01101_00023_nis	F200W	NISRAPID	5	1	1
jw01088001001_01101_00001_nis	F150W	NISRAPID	5	3	1
jw01088001001_01101_00002_nis	F150W	NISRAPID	5	3	2
jw01088001001_01101_00003_nis	F150W	NISRAPID	5	3	3
jw01088001001_01101_00004_nis	F150W	NISRAPID	5	3	4
jw01088003001_01101_00002_nis	F200W	NISRAPID	5	1	1
jw01088003001_01101_00003_nis	F140M	NISRAPID	5	2	1
jw01088003001_01101_00004_nis	F158M	NISRAPID	5	2	1
jw01088003001_01101_00005_nis	F115W	NISRAPID	5	1	1
jw01088003001_01101_00006_nis	F090W	NISRAPID	5	1	1
jw01088003001_01101_00009_nis	F480M	NISRAPID	15	1	1
jw01088003001_01101_00010_nis	F380M	NISRAPID	15	1	1
jw01088003001_01101_00011_nis	F430M	NISRAPID	15	1	1
jw01088003001_01101_00012_nis	F356W	NISRAPID	15	1	1

jw01088003001_01101_00013_nis	F444W	NISRAPID	15	1	1
jw01088003001_01101_00014_nis	F277W	NISRAPID	15	1	1

4 Methods

Starting from the astrometric and photometric catalog of point sources in the JWST calibration field, we calculate the reference (X, Y) coordinates of the stars in each image. This is done in the exact same way as in the `Mirage` simulation package, using a combination of the standard WCS keywords in the FITS headers, which are derived from the Science Instrument Aperture File (SIAF), and the full distortion solution whose polynomial coefficients are in the NIRISS distortion reference file. Specifically, this calculation involves the following for each image:

1. Running the `AssignWcsStep` step of the JWST pipeline on the standard "_cal.fits" pipeline product;
2. Creating a "`DataModel`" from the output file created by step 1 mentioned above;
3. Applying the `meta.wcs.world_to_pixel` function to that `DataModel`, using the (RA, DEC) coordinates of the stars in the JWST calibration field as input.

From the resulting photometric catalog of stars in the Science coordinate frame of the image, we then perform two extra subselection steps:

1. We select stars within the actual footprint of the NIRISS detector, using an additional buffer of 20 pixels at each edge to avoid dealing with incomplete spatial coverage of PSFs during the measurements.
2. Stars with companions within a distance of 2 pixels are excluded from further analysis. We also ran our scripts with a larger avoidance distance of 10 pixels, and the results of the two runs were indistinguishable from each other.
3. Using the `synphot` package along with `WebbPSF`, we determine an appropriate magnitude limit to avoid saturated stars in the image in question. We also exclude regions in the image that are within a radius of 50 pixels of each saturated star, to avoid possible problems with the bright diffraction spikes of their PSFs.

This selection procedure yielded of order 3000 – 7000 stars in each image, uniformly distributed across the image. For each star in the final catalog for each image, we then measure centroids using the following algorithms (or Python "classes") available in the `photutils` package:

1. `photutils.centroids.centroid_com`, which determines the "center of mass" from image moments. Based on prior experience with similar algorithms (see Holfeltz et al. 2014), we consider measurement box sizes of 3, 5, and 7 pixels along each axis.
2. `photutils.centroids.centroid_2dg`, which fits a 2-D Gaussian (plus a constant) to the pixel values. We consider measurement box sizes of 5, 7, and 9 pixels.[†]
3. `photutils.centroids.centroid_quadratic`, which fits a 2-D quadratic function to the pixel values. We again consider measurement box sizes of 5, 7, and 9 pixels.
4. `photutils.detection.DAOStarFinder`, which provides an implementation of the DAOFIND algorithm of Stetson (1987). It finds local density maxima with a user-

[†] A box size of 3 pixels was also considered in this case, but it was found to cause problems with the Gaussian fits.

specified FWHM that have a peak intensity greater than a specified threshold, as well as a shape with a 'roundness' and 'sharpness' within user-specified limits. The centroids, roundness and sharpness are evaluated based on 1-D Gaussian fits to the intensity distributions along the X and Y axes.

5. `photutils.detection.IRAFStarFinder`, which implements IRAF's `starfind` algorithm. This is similar to `DAOStarFinder`, but it calculates centroids, roundness and sharpness using image moments rather than 1-D Gaussian fits.

After some testing, we ran the detection algorithms `DAOStarFinder` and `IRAFStarFinder` using the following input parameter values:

- `FWHM` = [1.10, 1.10, 1.10, 1.14, 1.17, 1.28, 1.70, 1.94, 2.03, 2.20, 2.22, 2.45] for imaging filter = ['f090w', 'f115w', 'f140m', 'f150w', 'f158w', 'f200w', 'f277w', 'f356w', 'f380m', 'f430m', 'f444w', 'f480m']. These FWHM values were determined from a set of `WebbPSF` PSFs, using an implementation of IRAF's `psfmeasure` algorithm, which measures "direct" (i.e., model-independent) FWHMs of the intensity profiles.
- `threshold = 20 * clipsig`, where `clipsig` is the standard deviation of 5–σ–clipped image statistics on the central (0.2 × NAXIS1, 0.2 × NAXIS2) pixels of the image.
- `sharplo = 0.0`, `sharphi = 3.0`, `roundlo = 0.0`, and `roundhi = 0.5`.

After each run of `DAOStarFinder` and `IRAFStarFinder`, the resulting X and Y coordinates of detections were matched to the input X and Y coordinates of the stars, and the closest detection was selected for each input star.

We also considered using the `Photutils` `ePSFBuilder` tools for building an effective PSF (ePSF) following the prescriptions of Anderson & King (2000) which is known to provide excellent photometry. However, this constitutes a lengthy process that requires visual inspection and manual selection to ensure stars are adequately isolated from other stars, cosmic rays, and detector artifacts, while we are looking for a relatively quick method that allows one to update SI-to-SI alignments and SIAF updates with fast turnaround times during JWST commissioning. Furthermore, the ePSF building procedure also involves recentering of all stars, and this recentering process uses one of the algorithms that are tested in this study. With this in mind, we postpone the analysis of the astrometric precision of the `ePSFBuilder` tools to a separate report after commissioning.

5 Results

5.1 Overall Statistics

Spatial offsets from the expected positions are plotted for each of the centroid algorithms and box sizes in Figures 1-36 (3 figures per imaging filter) for the NIS-013 data. (The results for the NIS-011b data are very similar.) There are three figure panels for each combination of algorithm and box size, showing (1) all stars, (2) stars positioned within 0.1 pixel in X and Y from pixel centers, and (3) stars positioned within 0.1 pixel in X and Y from pixel corners. Each figure panel also shows the 5-σ-clipped mean offset of the data along with its ±1σ error bars. Overall statistics for "all stars" are listed below in Table 2, both for the NIS-011b and the NIS-013 data.

Table 2: 5-σ clipped statistics on offsets (in pixels) from input positions for each filter, centroid method, and measurement box size. The formally most precise method is highlighted in red for each filter.

Filter	Centroid Method	Box Size	Mean Offset (dX, dY)		Standard Deviation (σ (dX), σ (dY))	
			NIS-011b	NIS-013	NIS-011b	NIS-013
F090W	Center of Mass	3	0.232, 0.288	0.234, 0.285	0.197, 0.201	0.198, 0.195
		5	0.108, 0.168	0.106, 0.165	0.106, 0.108	0.091, 0.087
		7	0.116, 0.184	0.098, 0.175	0.185, 0.176	0.092, 0.085
	2-D Gaussian	5	-0.023, 0.042	-0.021, 0.045	0.067, 0.063	0.070, 0.062
		7	-0.023, 0.040	-0.021, 0.043	0.071, 0.066	0.073, 0.064
		9	-0.023, 0.038	-0.021, 0.042	0.077, 0.071	0.074, 0.066
	Quadratic	5	-0.145, -0.064	-0.147, -0.062	0.253, 0.233	0.253, 0.231
		7	0.002, 0.015	0.002, 0.022	0.178, 0.174	0.180, 0.168
		9	-0.002, 0.010	-0.002, 0.020	0.178, 0.177	0.180, 0.168
	DAOStarFinder	N/A	-0.019, 0.034	-0.014, 0.042	0.256, 0.276	0.259, 0.278
	IRAFStarFinder	N/A	-0.012, 0.034	-0.009, 0.037	0.079, 0.070	0.079, 0.067
F115W	Center of Mass	3	0.228, 0.282	0.227, 0.278	0.194, 0.207	0.194, 0.200
		5	0.089, 0.142	0.085, 0.138	0.099, 0.092	0.084, 0.073
		7	0.093, 0.142	0.074, 0.130	0.167, 0.162	0.078, 0.075
	2-D Gaussian	5	-0.017, 0.042	-0.015, 0.044	0.060, 0.061	0.062, 0.061
		7	-0.016, 0.040	-0.015, 0.043	0.063, 0.063	0.065, 0.063
		9	-0.017, 0.039	-0.015, 0.042	0.066, 0.067	0.067, 0.064
	Quadratic	5	-0.125, -0.037	-0.125, -0.040	0.245, 0.235	0.237, 0.230
		7	-0.002, 0.016	-0.001, 0.023	0.173, 0.169	0.174, 0.163
		9	-0.003, 0.012	-0.004, 0.019	0.174, 0.169	0.174, 0.164
	DAOStarFinder	N/A	-0.016, 0.045	-0.012, 0.053	0.266, 0.280	0.269, 0.280
	IRAFStarFinder	N/A	-0.015, 0.044	-0.013, 0.046	0.070, 0.064	0.070, 0.062
F140M	Center of Mass	3	0.231, 0.285	0.236, 0.283	0.185, 0.200	0.188, 0.195
		5	0.079, 0.137	0.083, 0.140	0.091, 0.073	0.077, 0.056
		7	0.066, 0.112	0.063, 0.111	0.162, 0.158	0.068, 0.059
	2-D Gaussian	5	-0.011, 0.030	-0.010, 0.032	0.048, 0.051	0.049, 0.052
		7	-0.010, 0.030	-0.010, 0.031	0.051, 0.053	0.052, 0.053
		9	-0.011, 0.028	-0.010, 0.029	0.054, 0.058	0.054, 0.055
	Quadratic	5	-0.096, -0.022	-0.089, -0.025	0.254, 0.266	0.249, 0.255
		7	-0.006, 0.021	-0.006, 0.026	0.163, 0.161	0.163, 0.154
		9	-0.006, 0.014	-0.007, 0.020	0.164, 0.161	0.163, 0.154
	DAOStarFinder	N/A	-0.009, 0.043	-0.010, 0.050	0.271, 0.287	0.279, 0.286
	IRAFStarFinder	N/A	-0.013, 0.046	-0.012, 0.047	0.057, 0.046	0.055, 0.045
F150W	Center of Mass	3	0.240, 0.291	0.244, 0.290	0.183, 0.197	0.185, 0.193
		5	0.085, 0.140	0.087, 0.142	0.086, 0.068	0.073, 0.054
		7	0.068, 0.116	0.064, 0.114	0.142, 0.142	0.061, 0.057

	2-D Gaussian	5	-0.009, 0.025	-0.009, 0.026	0.044, 0.047	0.045, 0.047
		7	-0.009, 0.024	-0.008, 0.025	0.047, 0.049	0.047, 0.049
		9	-0.009, 0.023	-0.009, 0.025	0.048, 0.050	0.050, 0.050
	Quadratic	5	-0.079, -0.016	-0.083, -0.031	0.247, 0.271	0.253, 0.270
		7	-0.006, 0.023	-0.005, 0.028	0.158, 0.157	0.159, 0.151
		9	-0.006, 0.016	-0.006, 0.020	0.159, 0.157	0.158, 0.150
	DAOStarFinder	N/A	-0.007, 0.036	-0.008, 0.043	0.228, 0.238	0.233, 0.240
	IRAFStarFinder	N/A	-0.013, 0.044	-0.011, 0.045	0.051, 0.041	0.051, 0.039
F158M	Center of Mass	3	0.242, 0.294	0.247, 0.292	0.175, 0.191	0.178, 0.184
		5	0.082, 0.137	0.088, 0.141	0.080, 0.064	0.069, 0.048
		7	0.063, 0.112	0.060, 0.113	0.144, 0.139	0.056, 0.054
	2-D Gaussian	5	-0.008, 0.019	-0.007, 0.019	0.039, 0.042	0.040, 0.042
		7	-0.008, 0.018	-0.007, 0.019	0.042, 0.043	0.043, 0.043
		9	-0.007, 0.016	-0.006, 0.018	0.044, 0.046	0.045, 0.054
	Quadratic	5	-0.069, -0.011	-0.077, -0.029	0.252, 0.277	0.257, 0.276
		7	-0.008, 0.026	-0.008, 0.029	0.153, 0.152	0.153, 0.147
		9	-0.008, 0.018	-0.009, 0.022	0.152, 0.152	0.153, 0.146
	DAOStarFinder	N/A	-0.003, 0.026	-0.005, 0.032	0.200, 0.211	0.204. 0.211
	IRAFStarFinder	N/A	-0.012, 0.043	-0.011, 0.044	0.046, 0.037	0.046, 0.034
F200W	Center of Mass	3	0.282, 0.328	0.287, 0.330	0.168, 0.182	0.173, 0.182
		5	0.099, 0.135	0.102. 0.137	0.068, 0.056	0.056, 0.039
		7	0.063, 0.131	0.053, 0.124	0.144, 0.144	0.047, 0.047
	2-D Gaussian	5	-0.003, -0.003	-0.002, -0.004	0.016, 0.017	0.017, 0.018
		7	-0.002, -0.004	-0.002, -0.004	0.020, 0.019	0.021, 0.020
		9	-0.002, -0.005	-0.002, -0.004	0.021, 0.020	0.023, 0.021
	Quadratic	5	-0.015, -0.000	-0.020, -0.033	0.255, 0.286	0.262, 0.305
		7	-0.006, 0.032	-0.003, 0.037	0.140, 0.144	0.204, 0.349
		9	-0.006, 0.025	-0.003, 0.030	0.140, 0.144	0.141, 0.138
	DAOStarFinder	N/A	-0.000, 0.003	0.000, 0.006	0.140, 0.150	0.145, 0.151
	IRAFStarFinder	N/A	-0.009, 0.033	-0.009, 0.033	0.032, 0.026	0.033, 0.025
F277W	Center of Mass	3	0.407, 0.437	0.411, 0.439	0.204, 0.218	0.206, 0.213
		5	0.201, 0.227	0.205, 0.232	0.082, 0.083	0.053, 0.054
		7	0.102, 0.163	0.089, 0.149	0.212, 0.214	0.080, 0.072
	2-D Gaussian	5	0.000, -0.007	0.001, -0.008	0.018, 0.017	0.018, 0.016
		7	-0.000, -0.008	0.000, -0.008	0.014, 0.014	0.014, 0.012
		9	-0.001, -0.009	-0.000, -0.008	0.010, 0.008	0.011, 0.010
	Quadratic	5	0.027, 0.014	0.029, -0.016	0.268, 0.286	0.259, 0.296
		7	-0.009, 0.022	-0.007, 0.031	0.154, 0.151	0.152, 0.141
		9	-0.010, 0.020	-0.009, 0.028	0.154, 0.151	0.152, 0.141
	DAOStarFinder	N/A	-0.001, -0.009	0.001, -0.007	0.068, 0.068	0.068, 0.066

	IRAFStarFinder	N/A	-0.009, 0.009	-0.008, 0.011	0.020, 0.023	0.017, 0.019
F356W	Center of Mass	3	0.433, 0.439	0.442, 0.447	0.209, 0.218	0.212, 0.213
		5	0.239, 0.255	0.251, 0.268	0.109, 0.116	0.085, 0.091
		7	0.205, 0.231	0.203, 0.225	0.239, 0.240	0.096, 0.082
	2-D Gaussian	5	-0.003, -0.008	-0.002, -0.008	0.019, 0.018	0.020, 0.017
		7	-0.001, -0.006	0.000, -0.006	0.017, 0.017	0.016, 0.014
		9	-0.001, -0.006	-0.000, -0.006	0.015, 0.014	0.016, 0.013
	Quadratic	5	-0.071, -0.089	-0.079, -0.122	0.307, 0.307	0.294, 0.320
		7	-0.003, 0.002	0.000, 0.011	0.163, 0.157	0.159, 0.147
		9	-0.005, 0.001	-0.001, 0.009	0.163, 0.156	0.160, 0.146
	DAOStarFinder	N/A	-0.002, -0.008	-0.001, -0.006	0.063, 0.062	0.061, 0.057
	IRAFStarFinder	N/A	-0.001, -0.009	0.000, -0.009	0.023, 0.024	0.021, 0.021
F380M	Center of Mass	3	0.437, 0.439	0.448, 0.447	0.199, 0.207	0.204, 0.201
		5	0.241, 0.253	0.253, 0.265	0.126, 0.132	0.104, 0.107
		7	0.246, 0.258	0.237, 0.250	0.248, 0.253	0.097, 0.088
	2-D Gaussian	5	-0.006, -0.010	-0.005, -0.010	0.021, 0.020	0.021, 0.019
		7	-0.001, -0.006	-0.000, -0.006	0.020, 0.020	0.018, 0.016
		9	-0.002, -0.006	-0.000, -0.006	0.018, 0.018	0.017, 0.015
	Quadratic	5	-0.123, -0.130	-0.127, -0.184	0.313, 0.298	0.296, 0.331
		7	-0.000, -0.001	0.007, 0.005	0.152, 0.152	0.149, 0.141
		9	-0.005, -0.004	0.003, 0.003	0.153, 0.153	0.149, 0.140
	DAOStarFinder	N/A	-0.002, -0.007	-0.002, -0.005	0.058, 0.057	0.055, 0.053
	IRAFStarFinder	N/A	-0.001, -0.009	0.000, -0.009	0.035, 0.035	0.033, 0.031
F430M	Center of Mass	3	0.460, 0.459	0.470, 0.467	0.183, 0.187	0.188, 0.185
		5	0.229, 0.234	0.242, 0.247	0.147, 0.148	0.129, 0.129
		7	0.281, 0.279	0.274, 0.276	0.240, 0.240	0.111, 0.104
	2-D Gaussian	5	-0.010, -0.012	-0.008, -0.012	0.025, 0.023	0.022, 0.019
		7	-0.002, -0.007	-0.000, -0.005	0.026, 0.026	0.019, 0.017
		9	-0.003, -0.007	-0.000, -0.005	0.024, 0.022	0.019, 0.017
	Quadratic	5	-0.198, -0.195	-0.203, -0.222	0.308, 0.303	0.282, 0.311
		7	0.000, -0.006	0.007, -0.000	0.132, 0.131	0.128, 0.122
		9	-0.003, -0.009	0.003, -0.003	0.131, 0.130	0.126, 0.121
	DAOStarFinder	N/A	-0.004, -0.007	-0.001, -0.003	0.050, 0.050	0.046, 0.042
	IRAFStarFinder	N/A	-0.002, -0.009	0.001, -0.008	0.031, 0.029	0.049, 0.048
F444W	Center of Mass	3	0.467, 0.464	0.481, 0.477	0.183, 0.187	0.188, 0.184
		5	0.223, 0.228	0.242, 0.245	0.145, 0.152	0.125, 0.127
		7	0.266, 0.269	0.271, 0.271	0.239, 0.249	0.104, 0.094
	2-D Gaussian	5	-0.009, -0.011	-0.007, -0.011	0.019, 0.018	0.018, 0.016
		7	-0.002, -0.007	-0.000, -0.006	0.021, 0.022	0.016, 0.014
		9	-0.002, -0.007	-0.000, -0.005	0.018, 0.018	0.015, 0.014

	Quadratic	5	-0.187, -0.196	-0.199, -0.224	0.295, 0.300	0.297, 0.305
		7	-0.002, -0.007	0.022, -0.000	0.128, 0.127	0.124, 0.116
		9	-0.004, -0.008	0.011, -0.001	0.128, 0.126	0.122, 0.115
	DAOStarFinder	N/A	-0.004, -0.006	-0.001, -0.004	0.047, 0.048	0.045, 0.041
	IRAFStarFinder	N/A	-0.002, -0.009	0.001, -0.008	0.026, 0.027	0.050, 0.048
F480M	Center of Mass	3	0.503, 0.501	0.517, 0.512	0.174, 0.176	0.182, 0.176
		5	0.205, 0.207	0.228, 0.225	0.159, 0.163	0.141, 0.142
		7	0.268, 0.267	0.275, 0.269	0.252, 0.259	0.119, 0.121
	2-D Gaussian	5	-0.009, -0.012	-0.008, -0.011	0.029, 0.028	0.025, 0.023
		7	-0.002, -0.008	-0.001, -0.006	0.031, 0.033	0.023, 0.020
		9	-0.002, -0.007	-0.000, -0.005	0.028, 0.029	0.022, 0.020
	Quadratic	5	-0.236, -0.263	-0.257, -0.263	0.300, 0.296	0.292, 0.298
		7	0.001, -0.005	0.007, 0.001	0.108, 0.110	0.104, 0.099
		9	-0.002, -0.009	0.003, -0.003	0.106, 0.110	0.104, 0.099
	DAOStarFinder	N/A	-0.004, -0.006	-0.001, -0.003	0.045, 0.047	0.039, 0.037
	IRAFStarFinder	N/A	-0.001, -0.009	0.002, -0.007	0.068, 0.035	0.067, 0.064

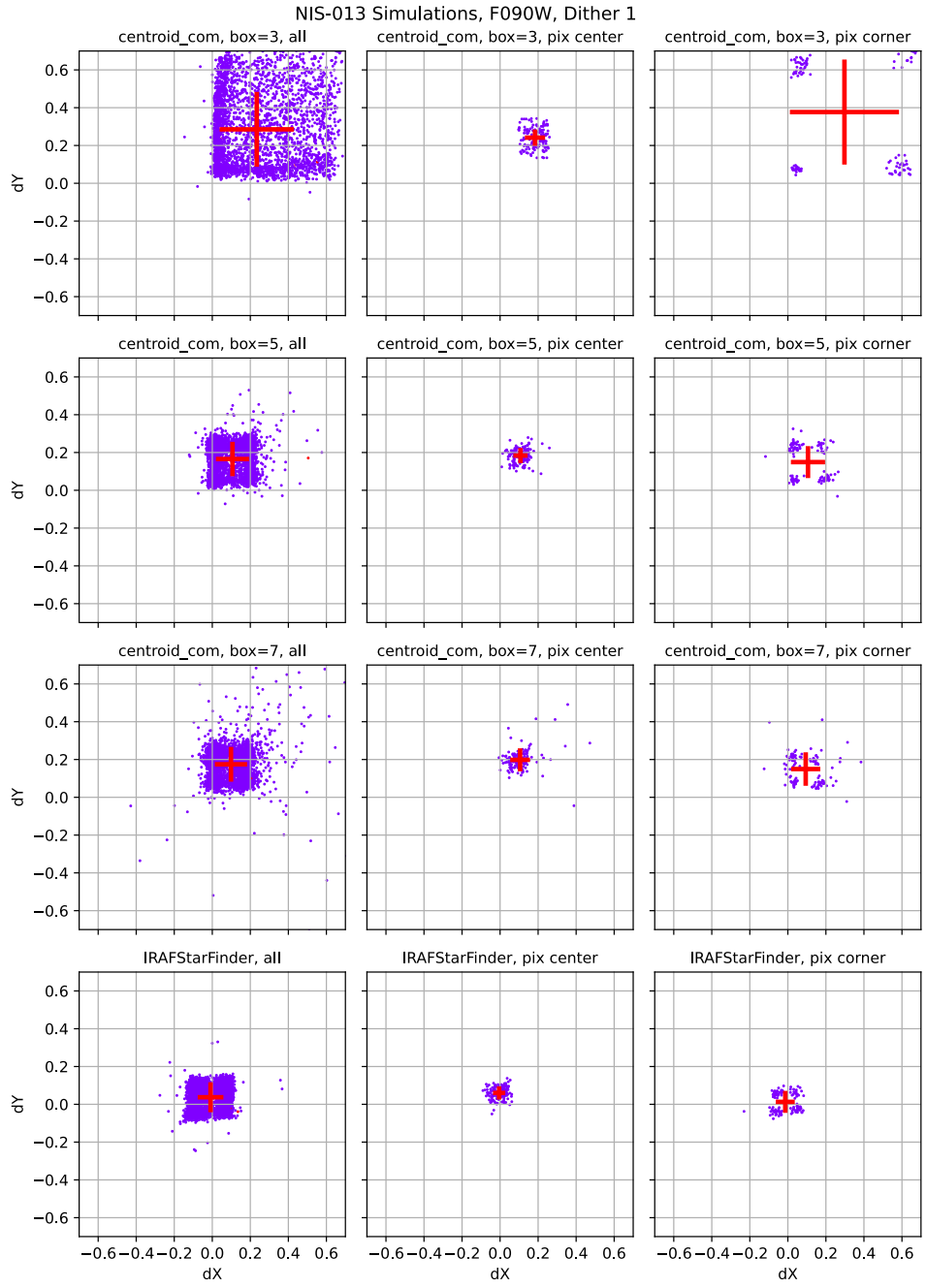

Figure 1: Scatter plots of spatial offsets (in pixels) from the input (X, Y) positions as measured by different centroiding algorithms. The centroiding algorithm and box size are indicated above every panel. Dots represent stars and the red error bars indicate the mean position and standard deviations in (X, Y) of all stars in the panel in question. The left-hand panels show all stars in the input list, the middle panels show stars placed within 0.1 pixel in X and Y from pixel centers, and the right-hand panels show stars placed within 0.1 pixel in X and Y from pixel corners. This Figure is for filter F090W.

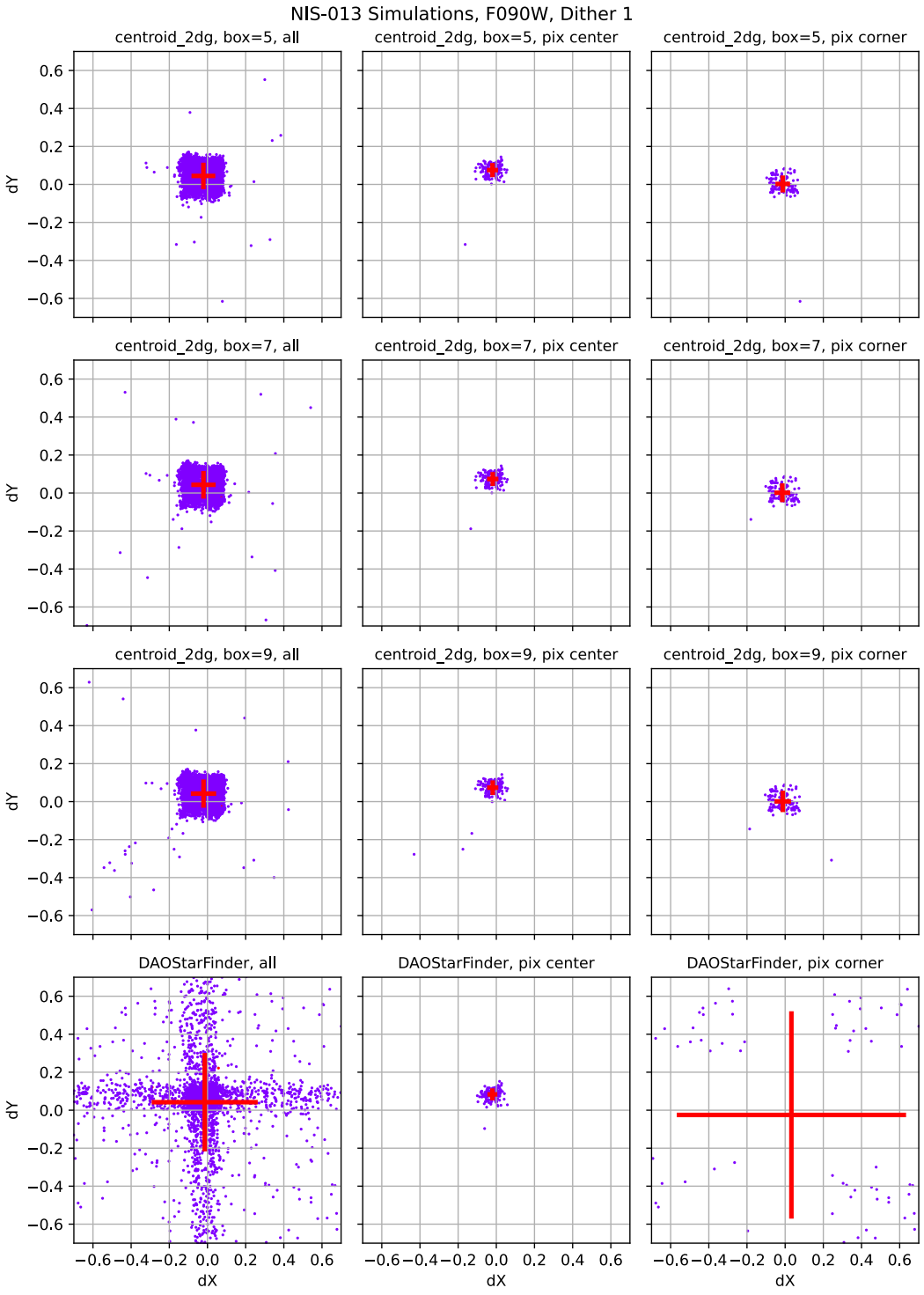

Figure 2: Same as Figure 1, but now for the 2-D Gaussian and DAOStarFinder centroiding algorithms.

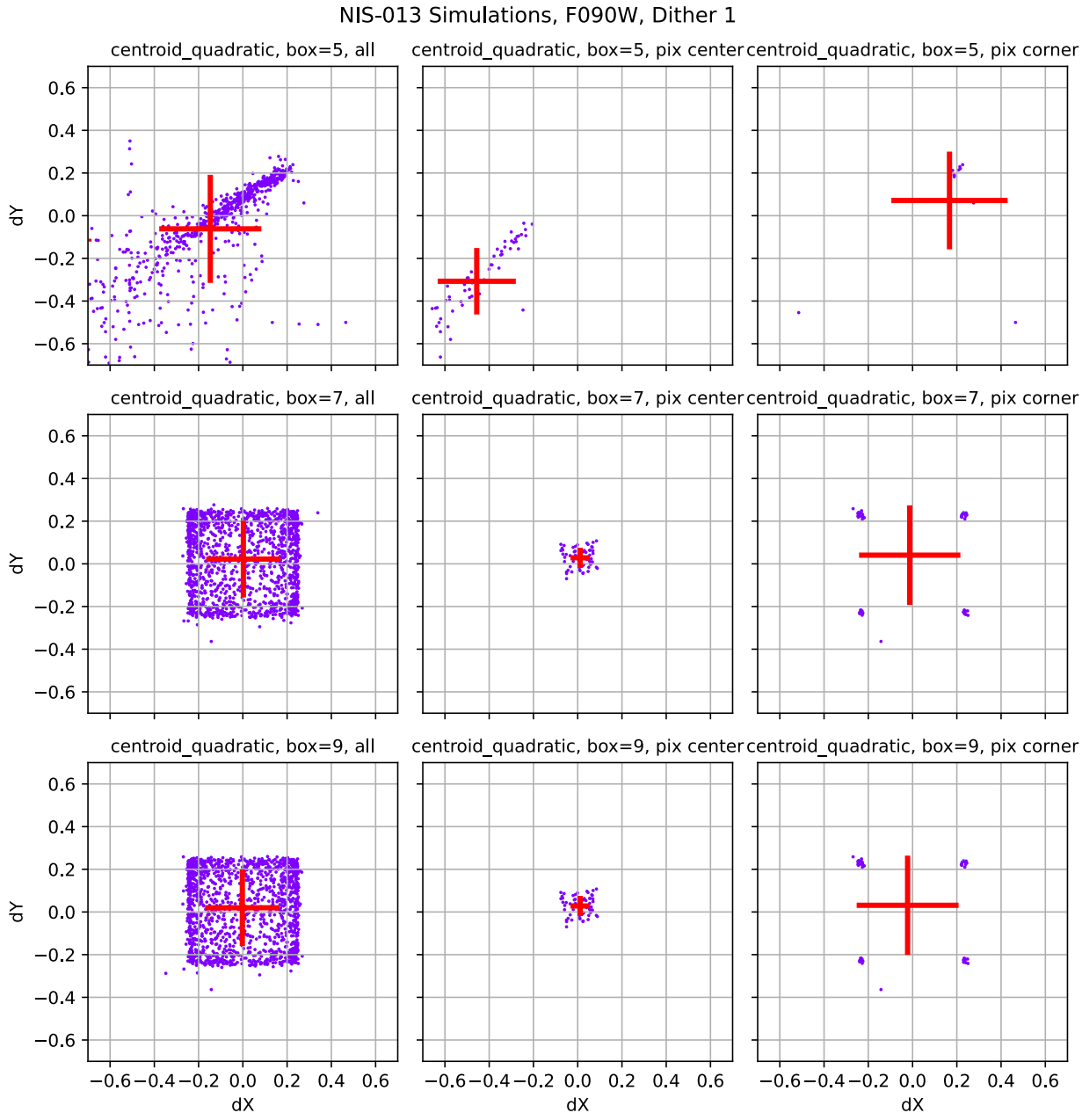

Figure 3: Same as Figure 1, but now for the Quadratic centroiding algorithm.

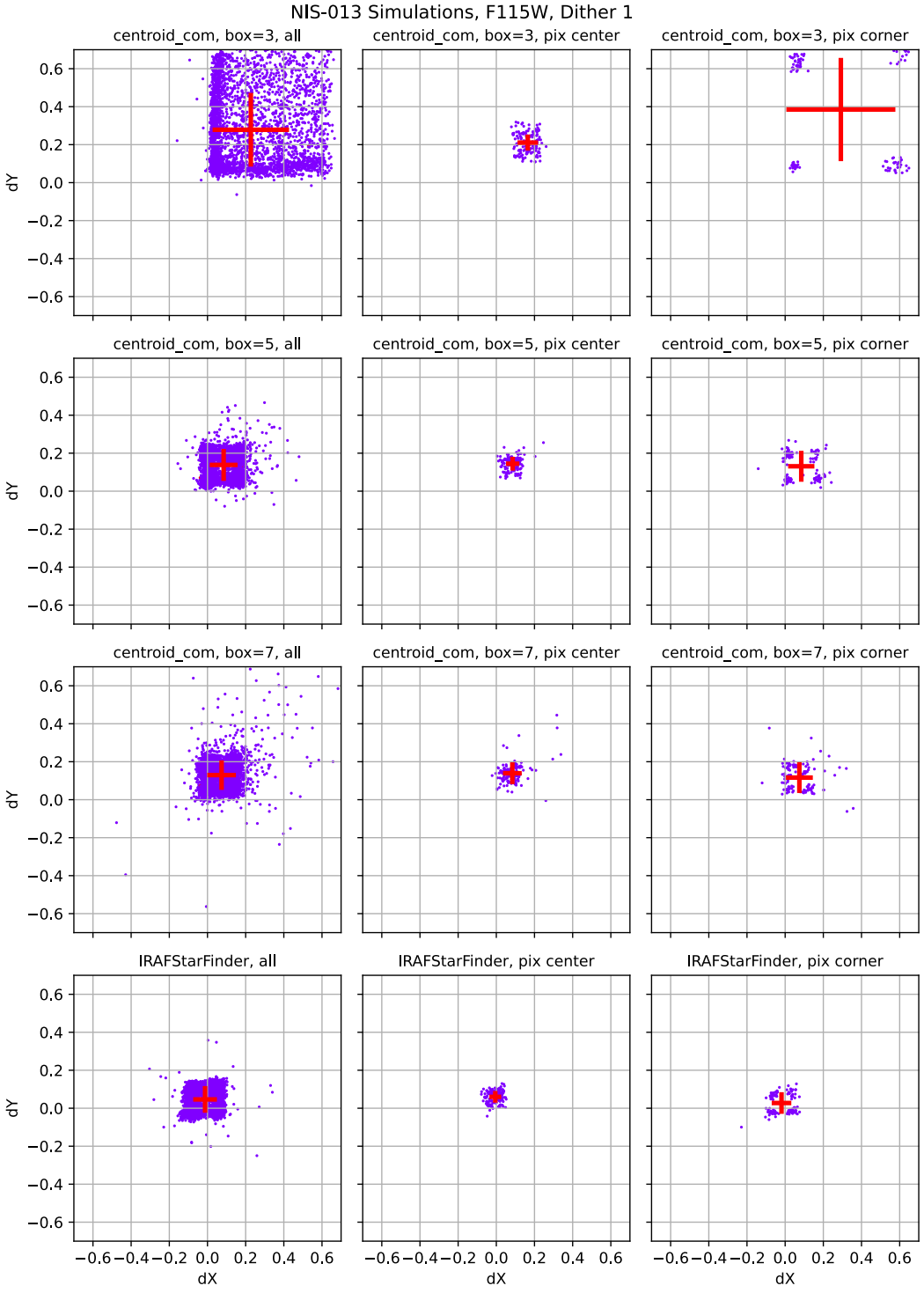

Figure 4: Same as Figure 1, but now for the F115W filter.

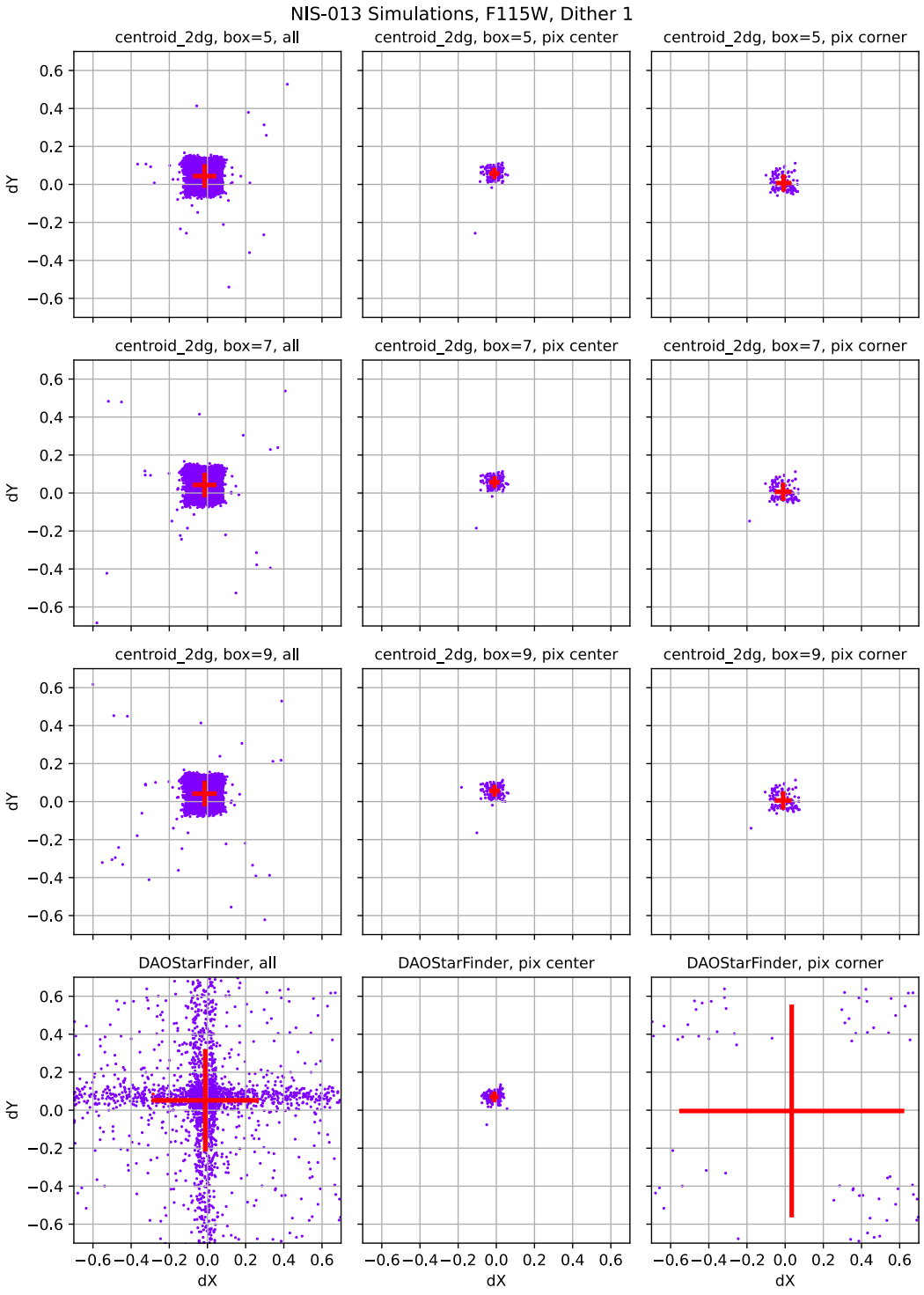

Figure 5: Same as Figure 2, but now for filter F115W.

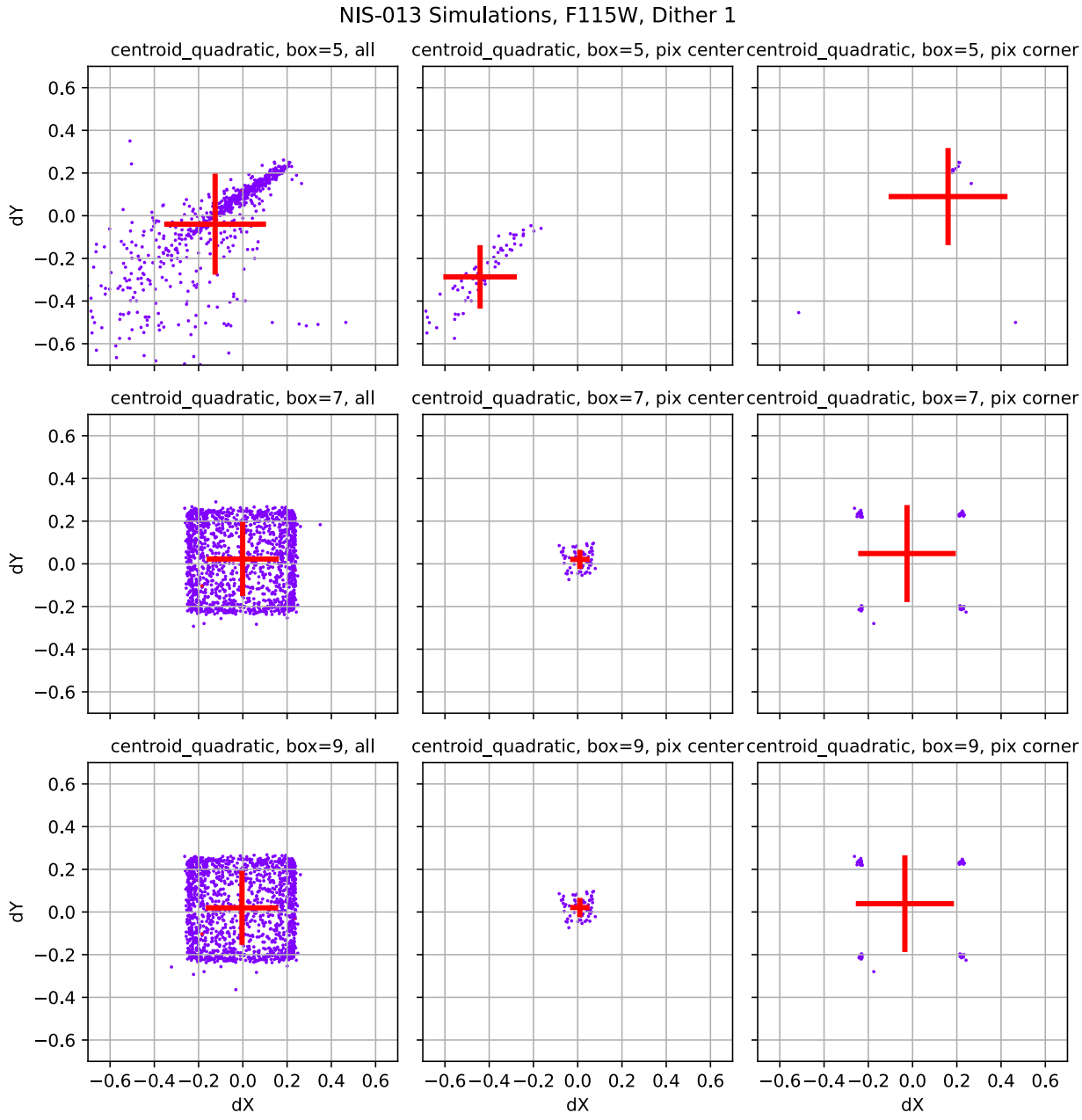

Figure 6: Same as Figure 3, but now for filter F115W.

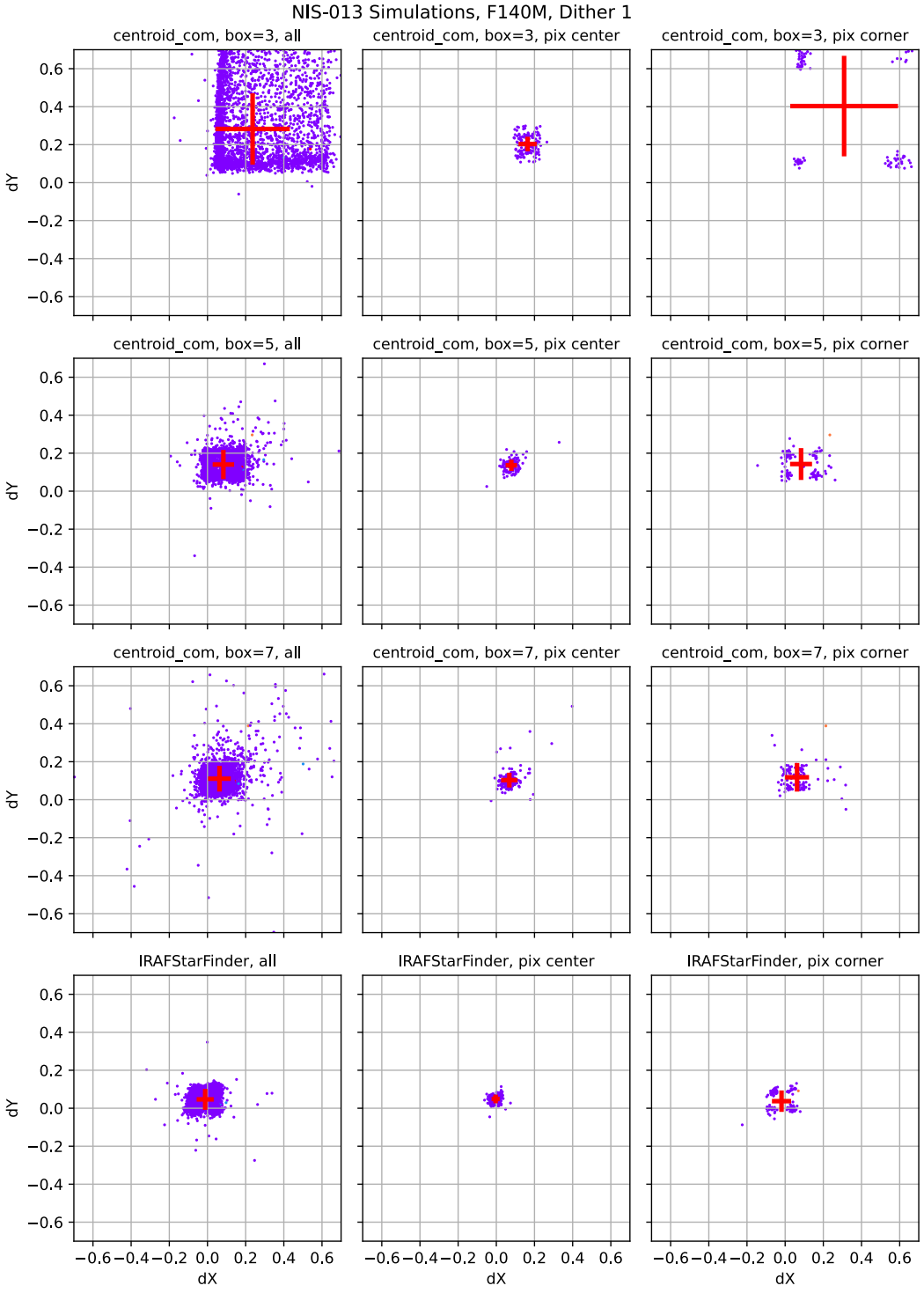

Figure 7: Same as Figure 1, but now for the F140M filter.

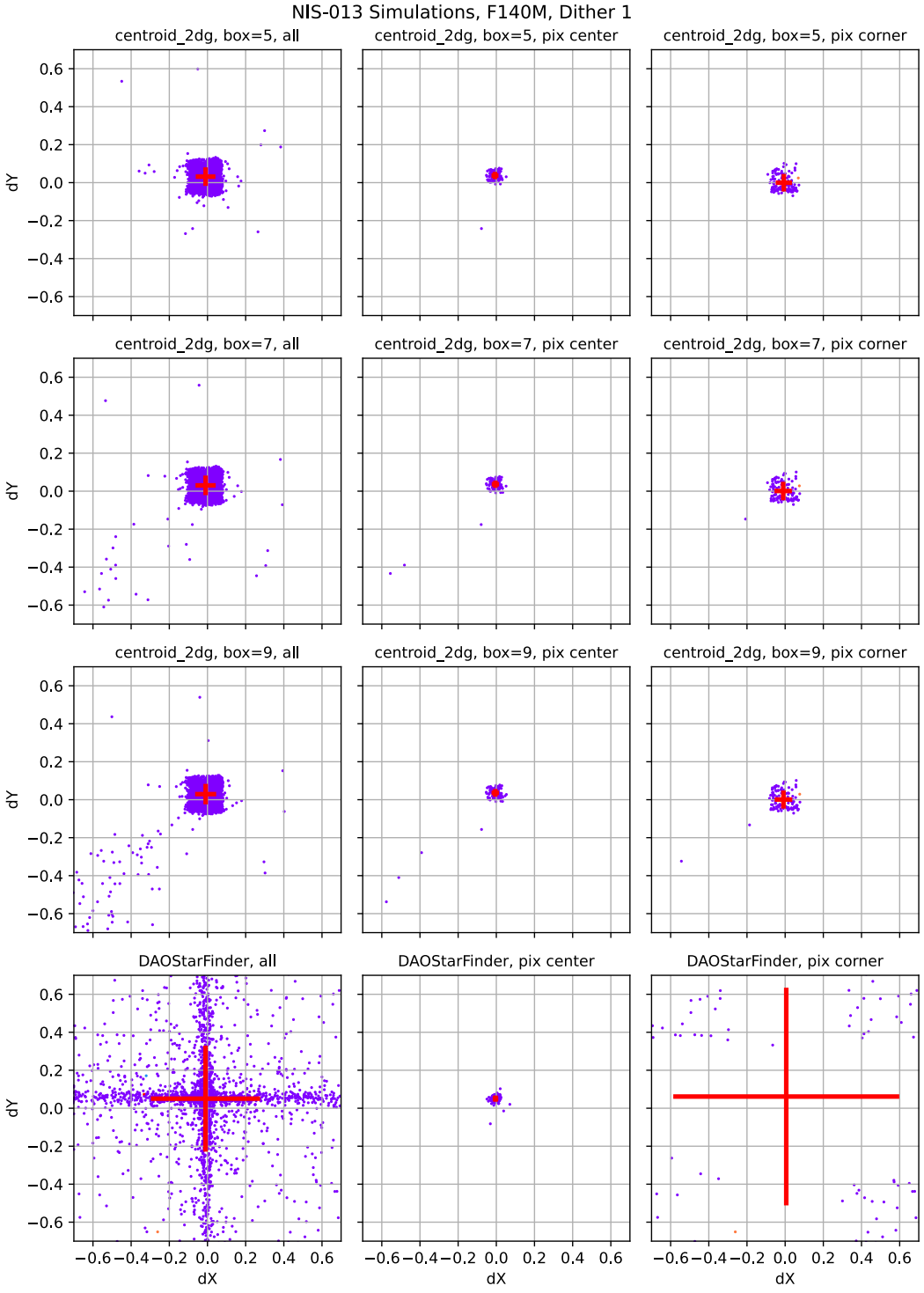

Figure 8: Same as Figure 2, but now for the F140M filter.

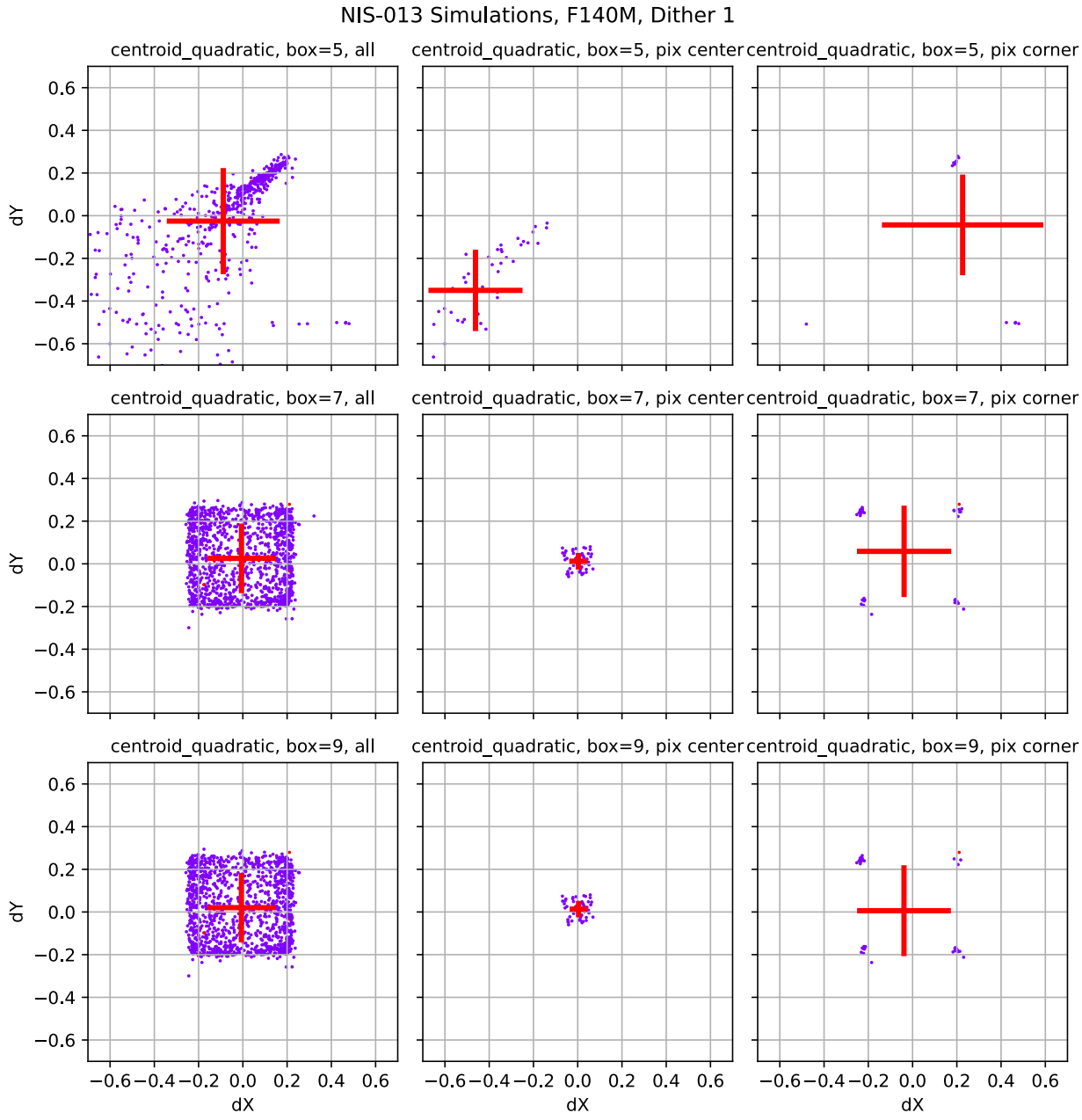

Figure 9: Same as Figure 3, but now for filter F140M.

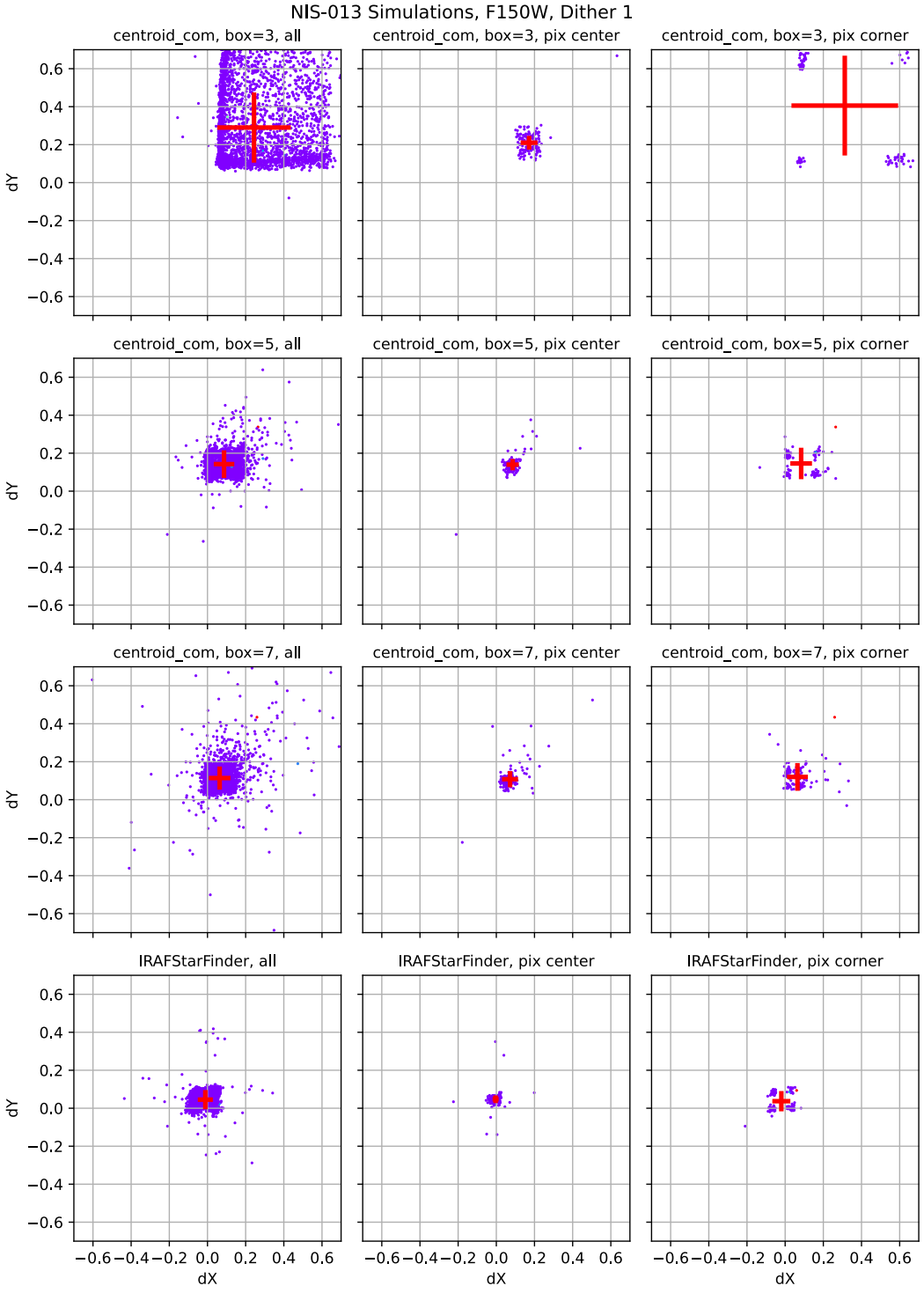

Figure 10: Same as Figure 1, but now for the F150W filter.

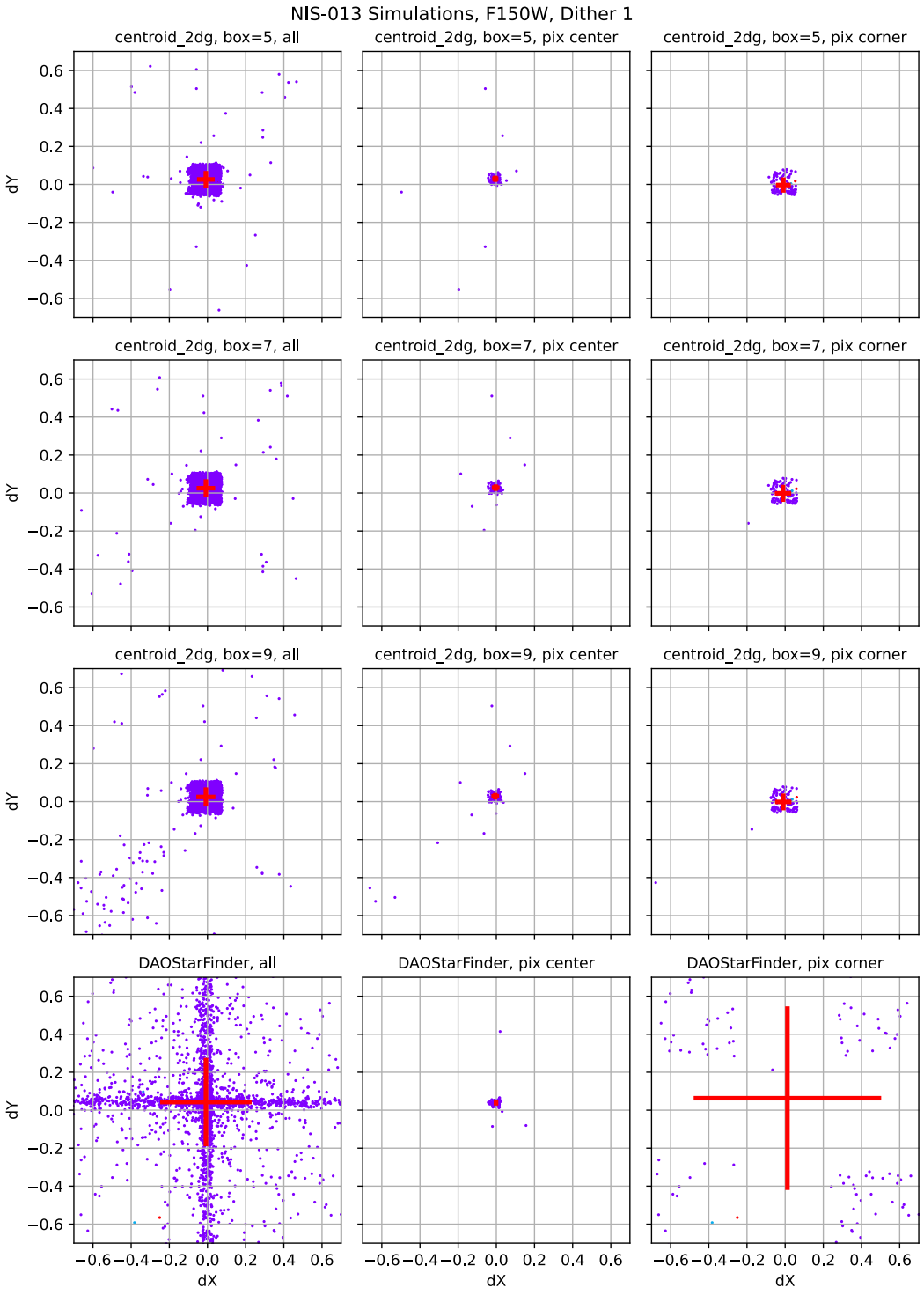

Figure 11: Same as Figure 2, but now for the F150W filter.

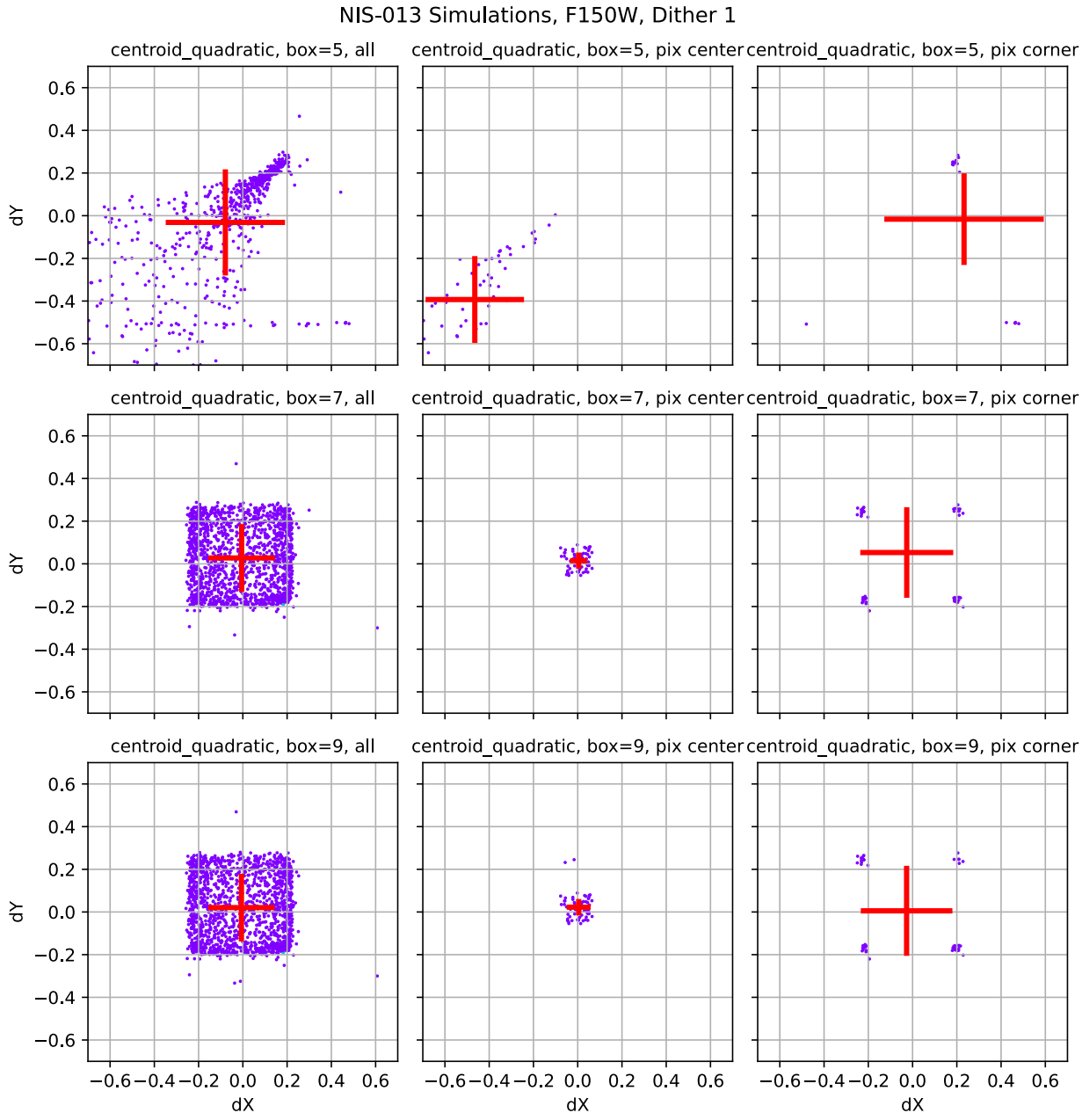

Figure 12: Same as Figure 3, but now for filter F150W.

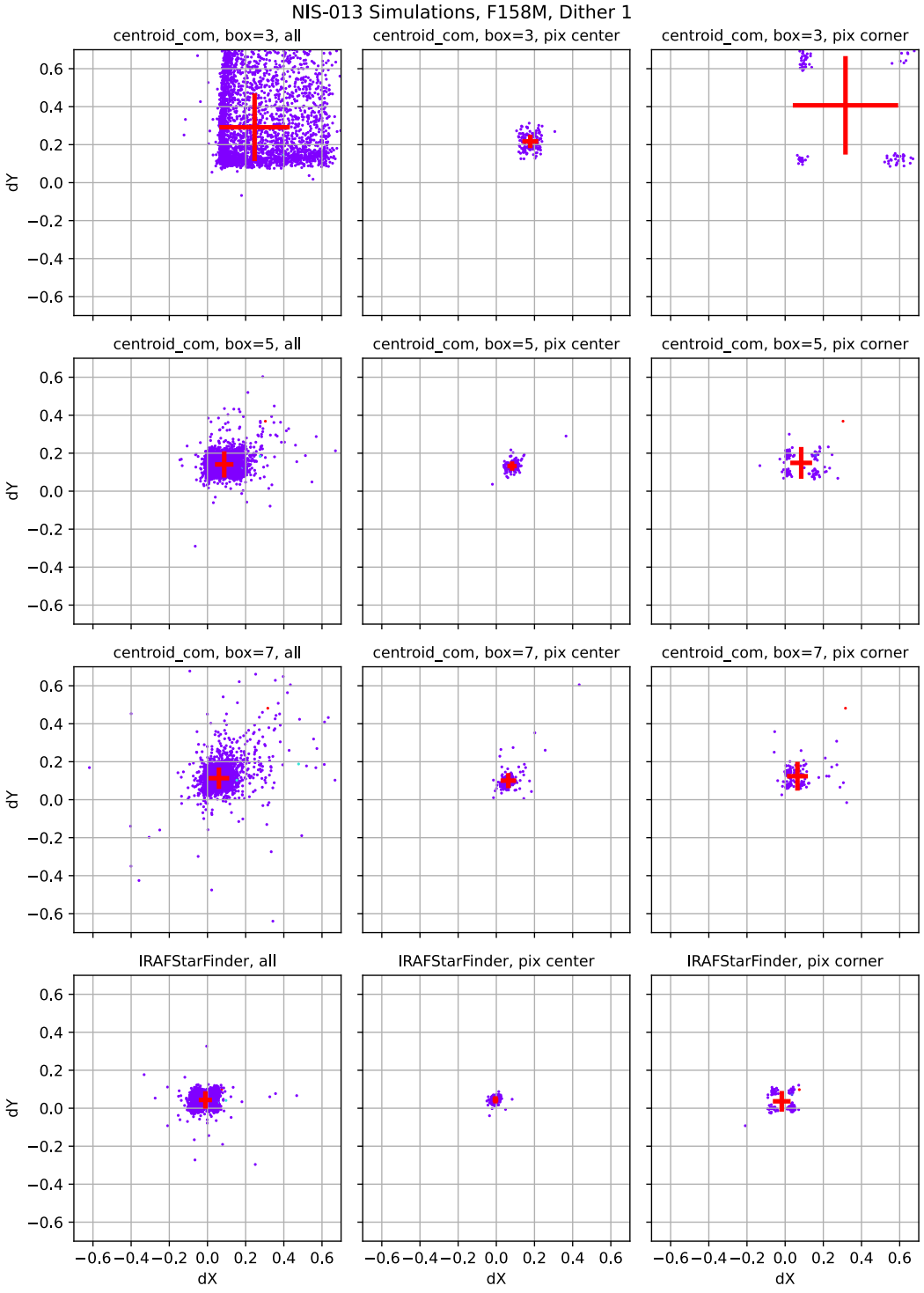

Figure 13: Same as Figure 1, but now for the F158M filter.

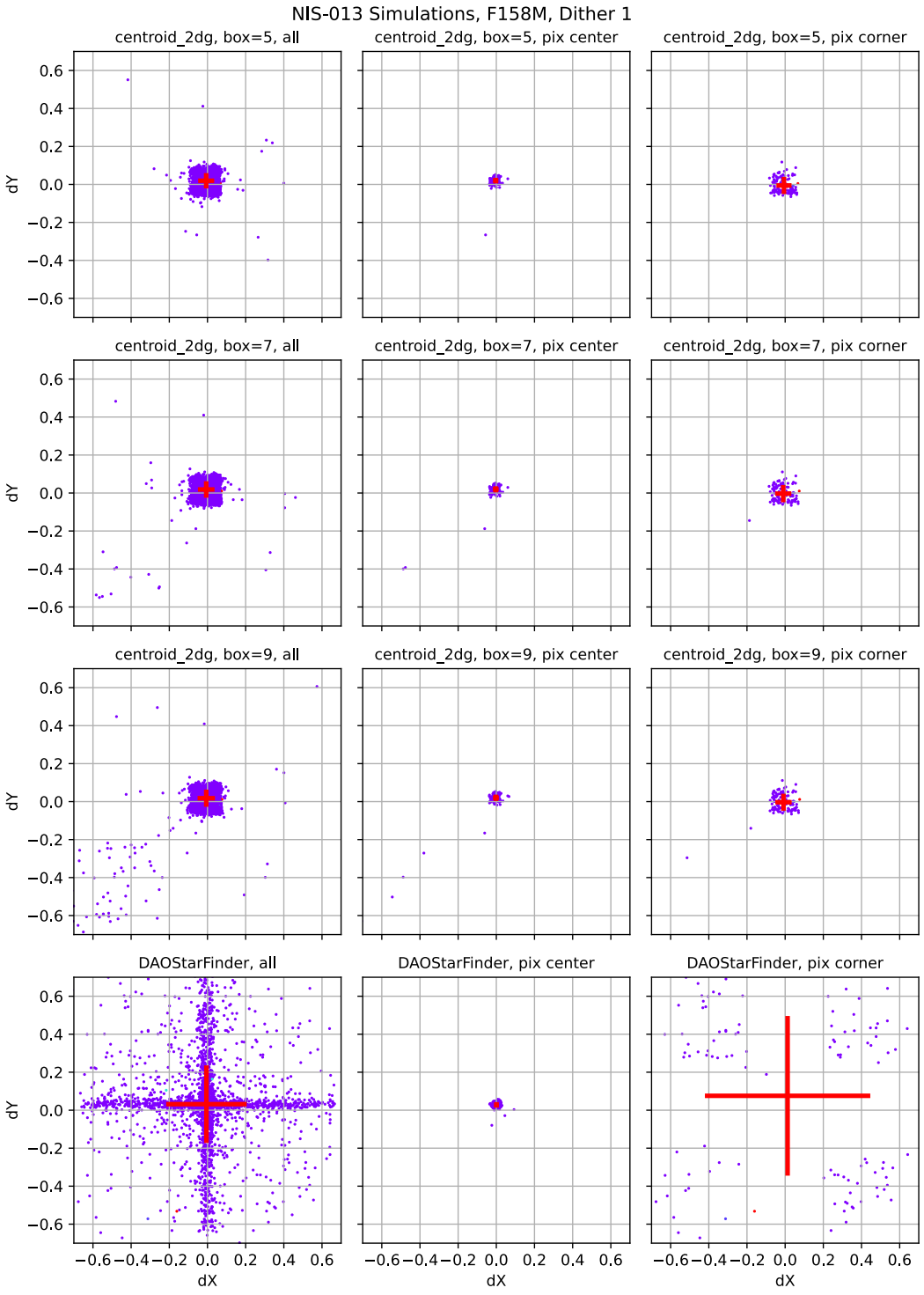

Figure 14: Same as Figure 2, but now for the F158M filter.

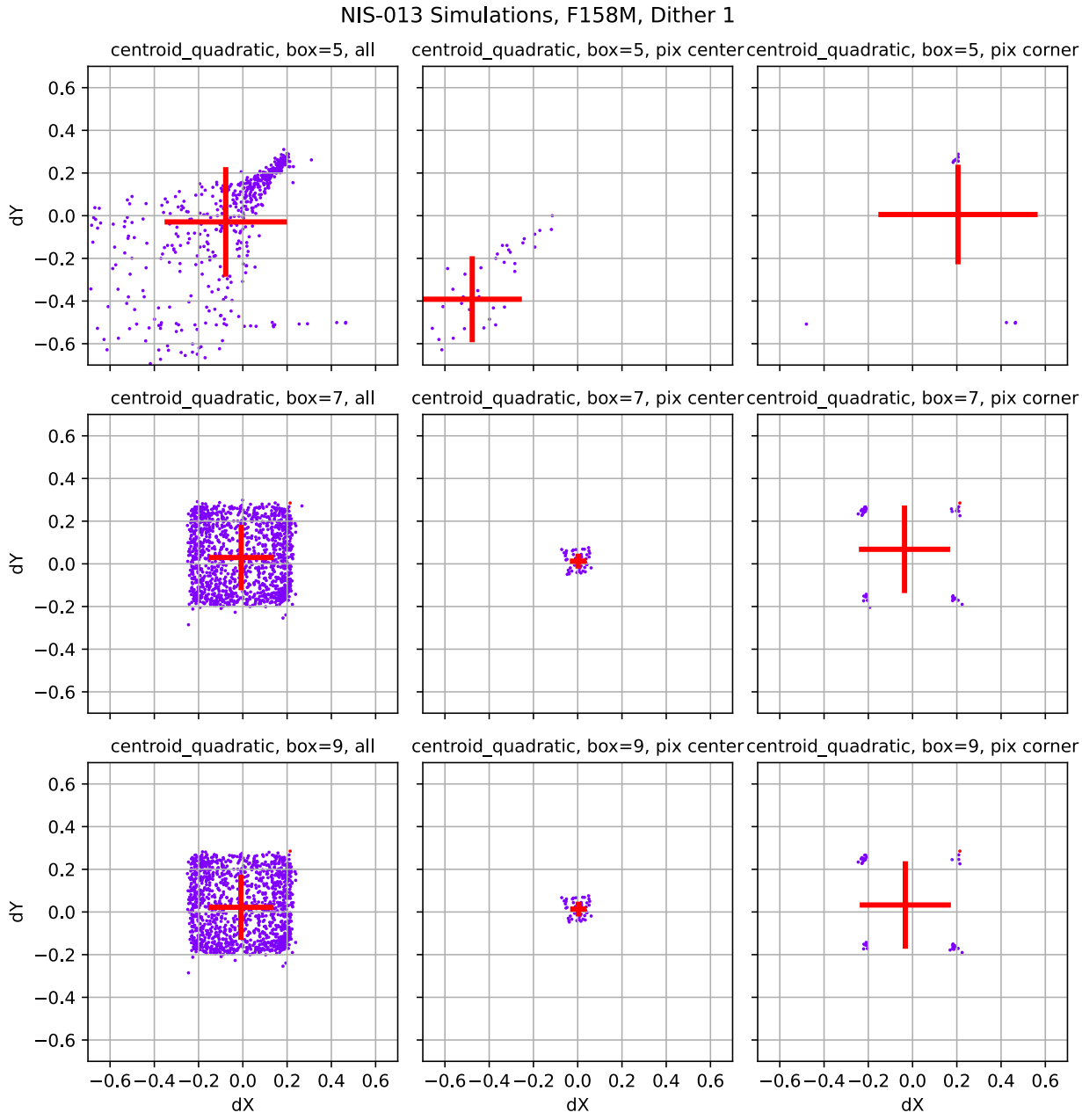

Figure 15: Same as Figure 3, but now for filter F158M.

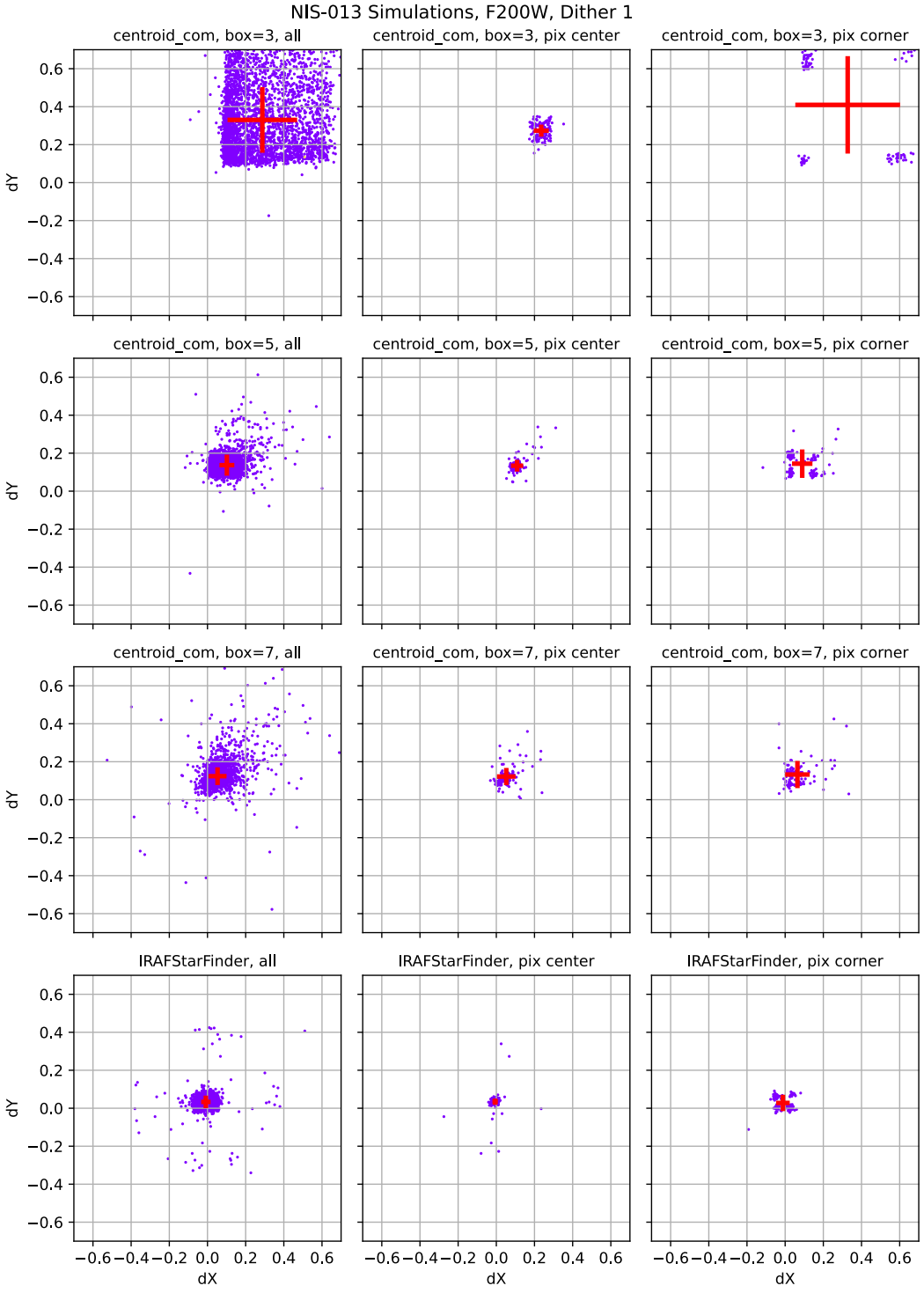

Figure 16: Same as Figure 1, but now for the F200W filter.

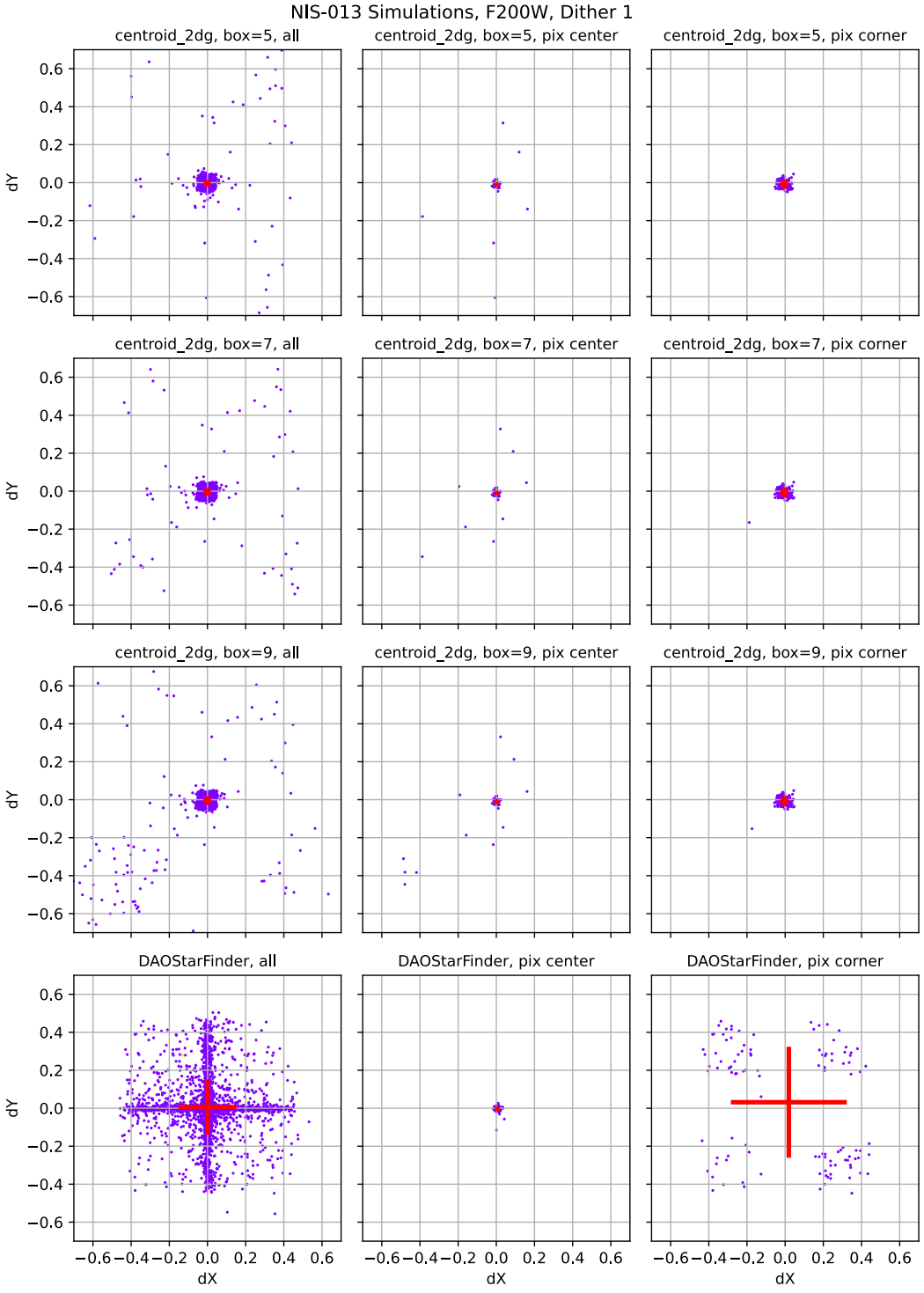

Figure 17: Same as Figure 2, but now for the F200W filter.

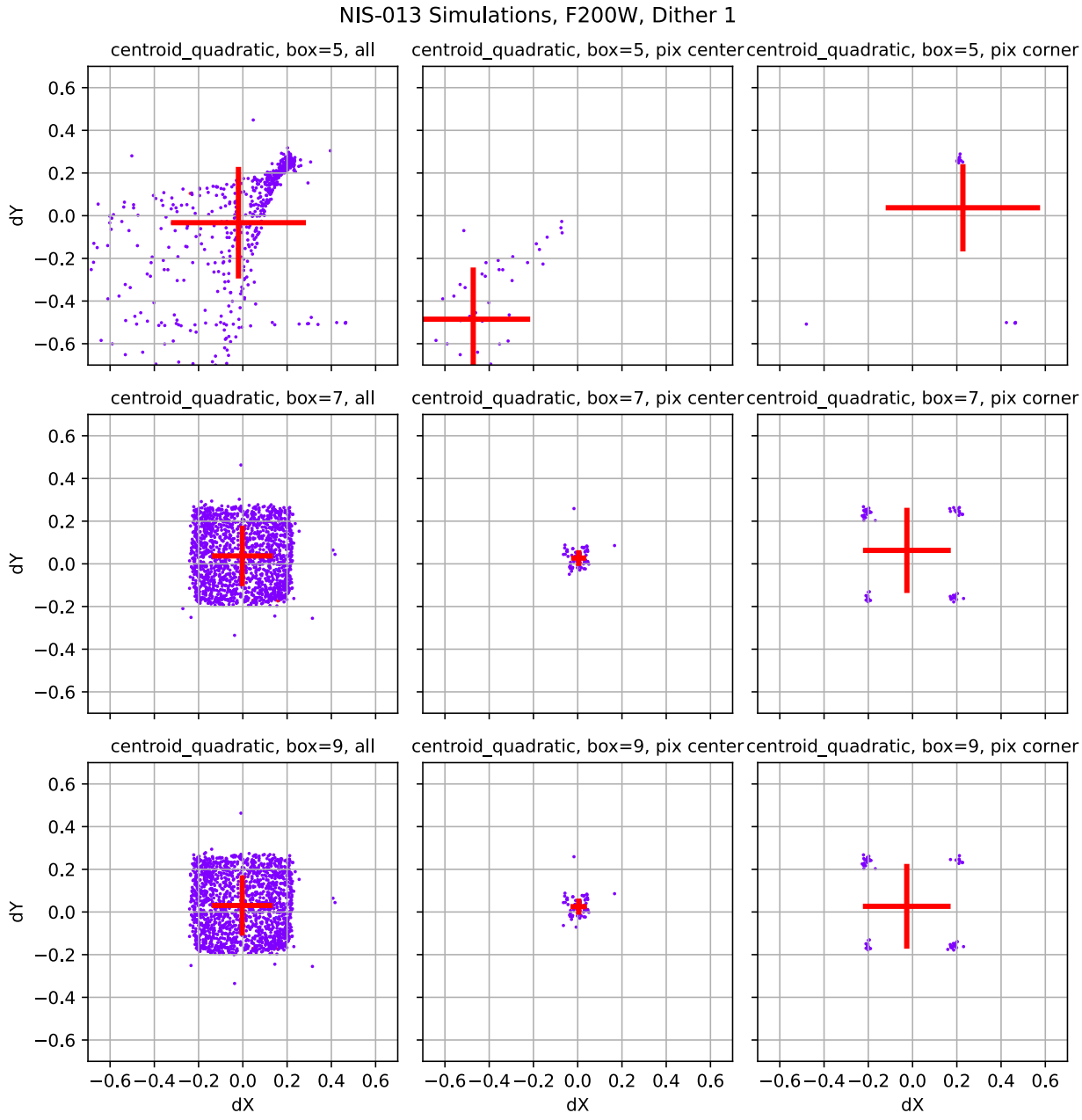

Figure 18: Same as Figure 3, but now for filter F200W.

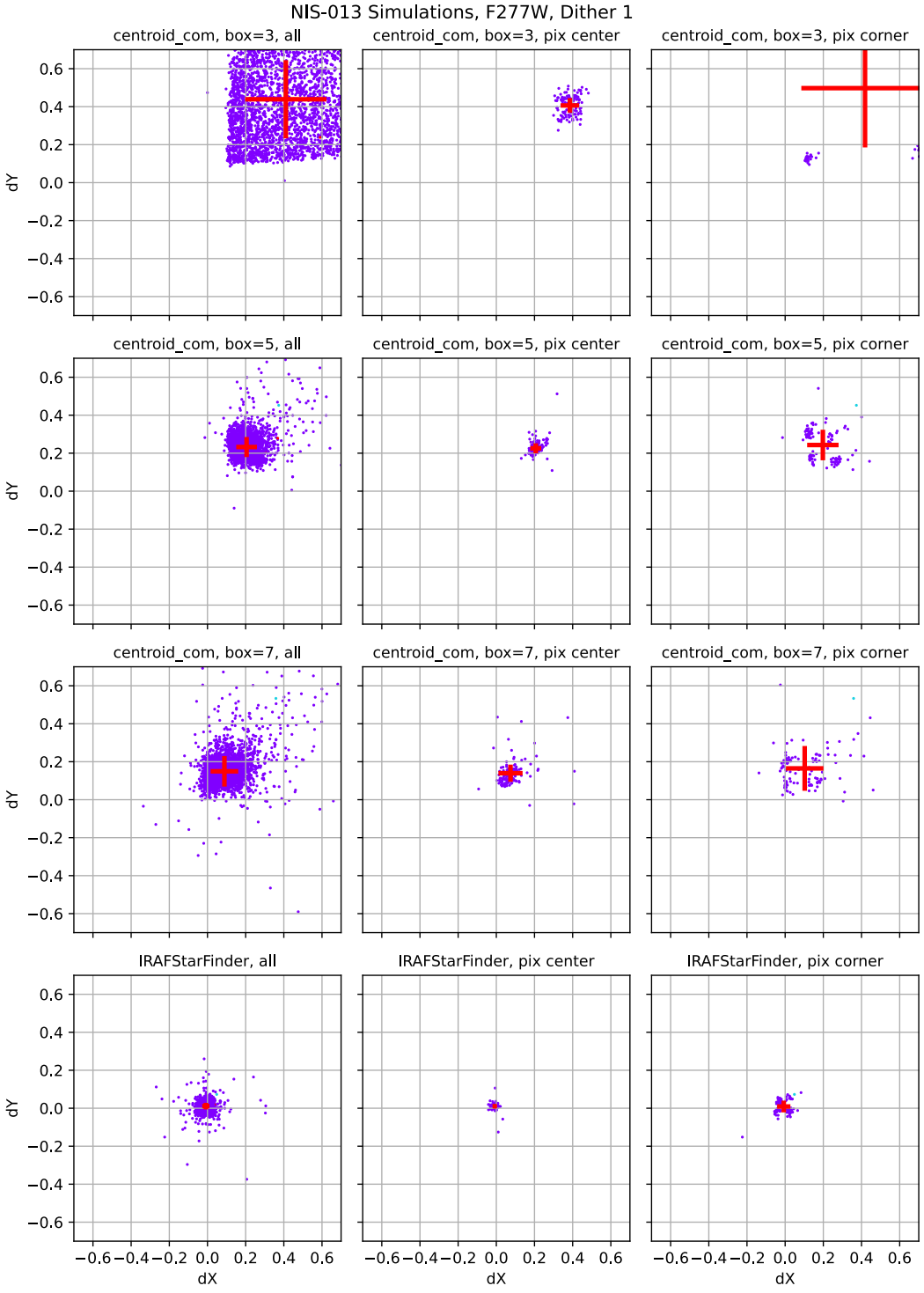

Figure 19: Same as Figure 1, but now for the F277W filter.

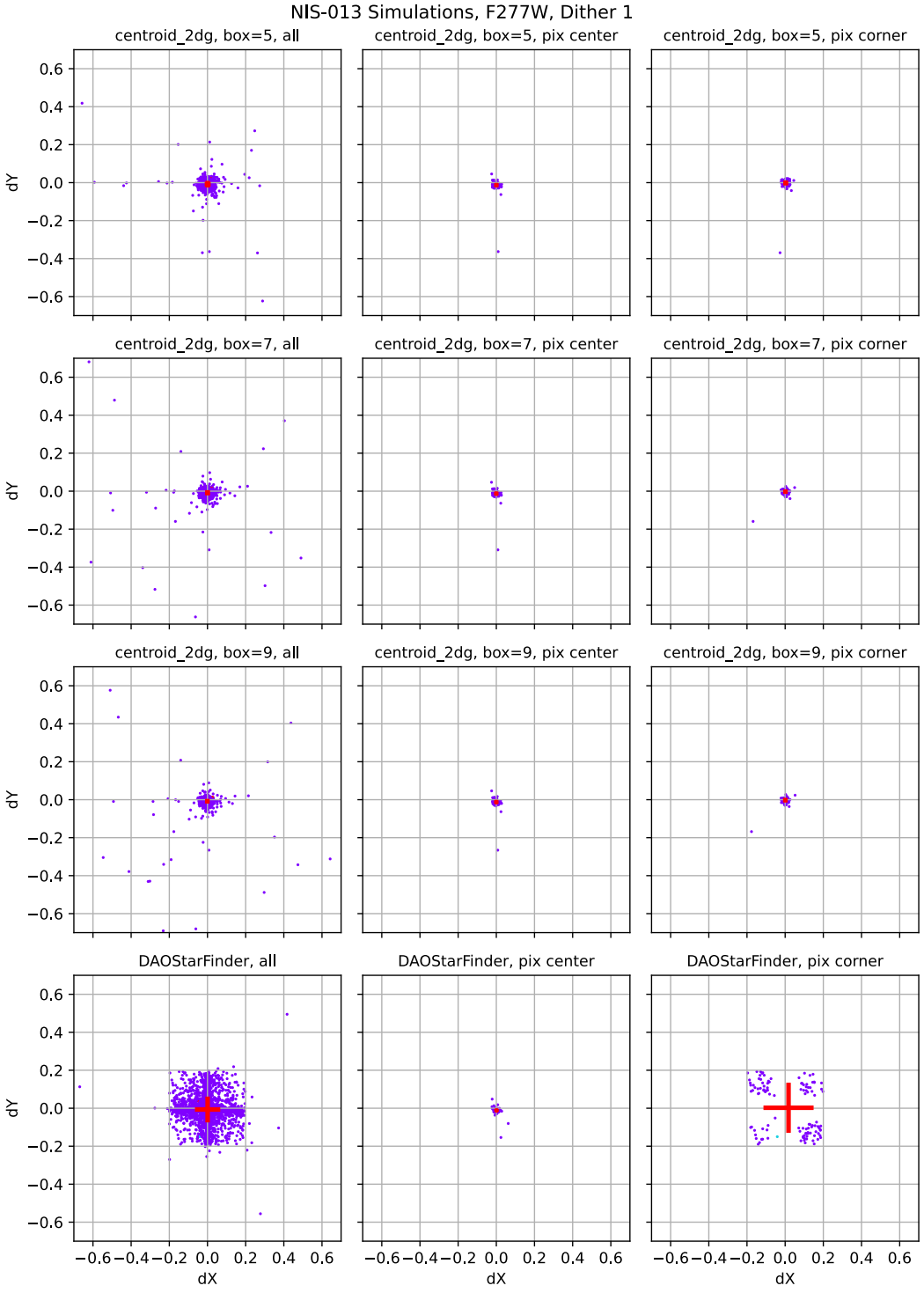

Figure 20: Same as Figure 2, but now for the F277W filter.

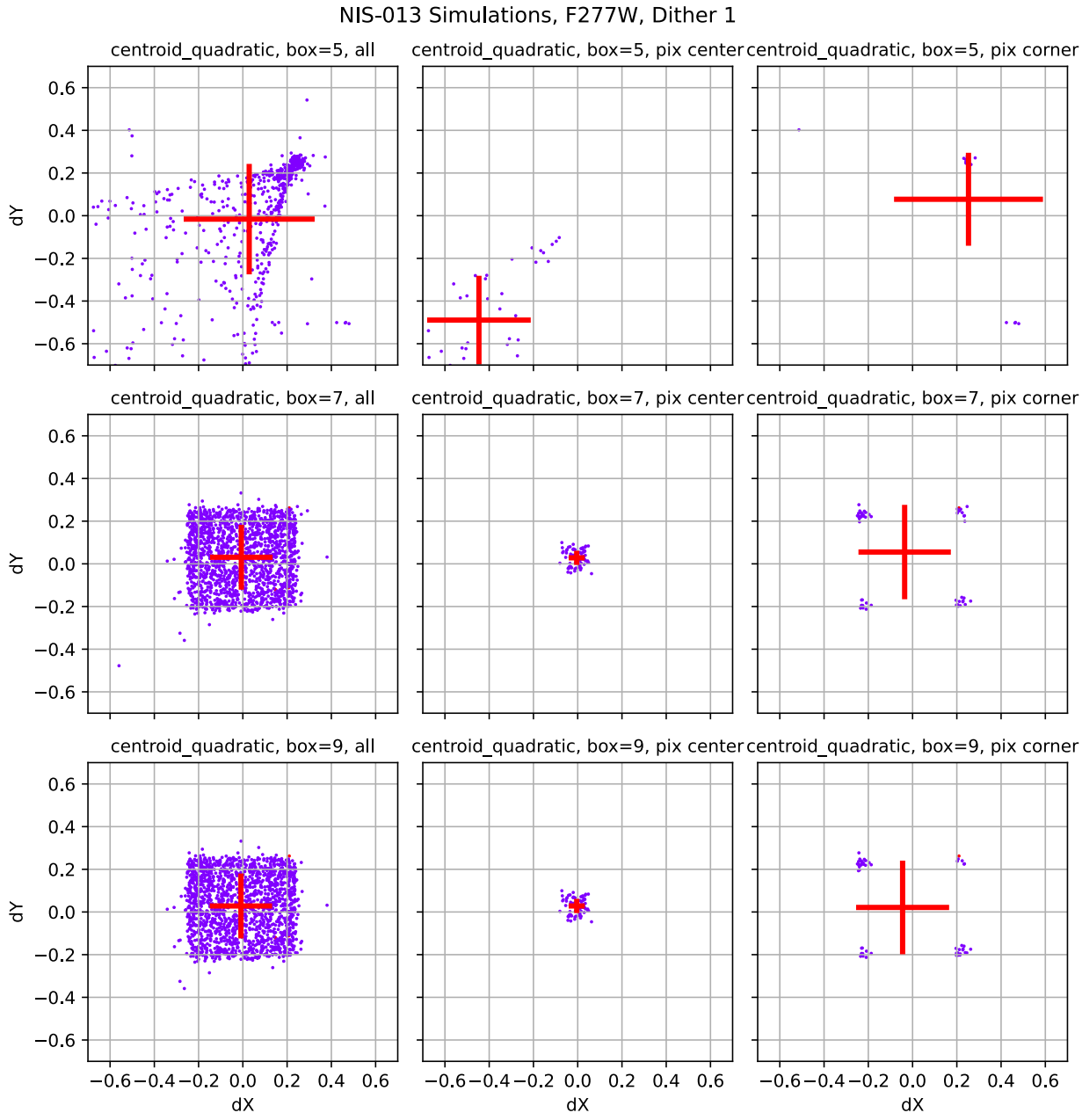

Figure 21: Same as Figure 3, but now for filter F277W.

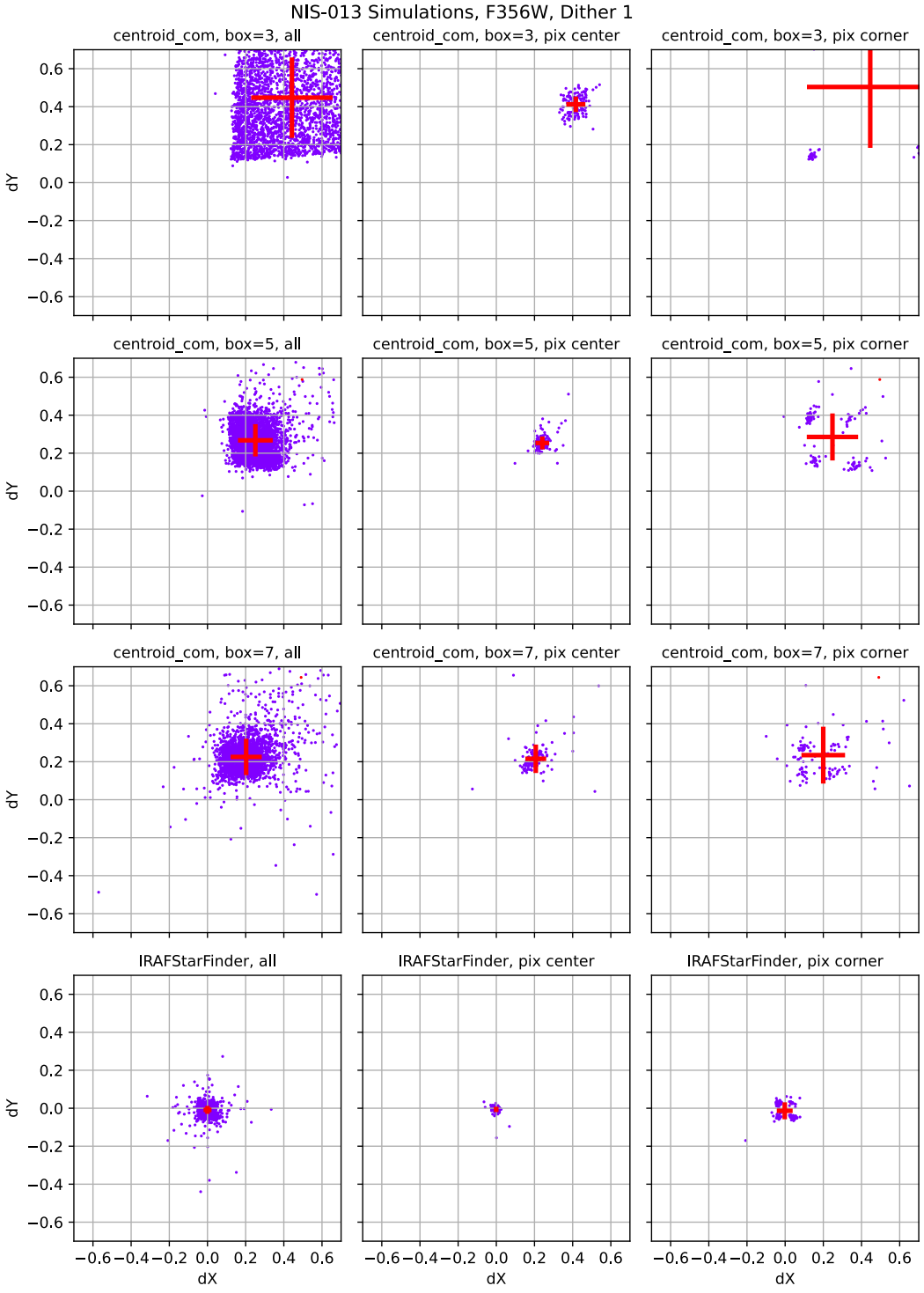

Figure 22: Same as Figure 1, but now for the F356W filter.

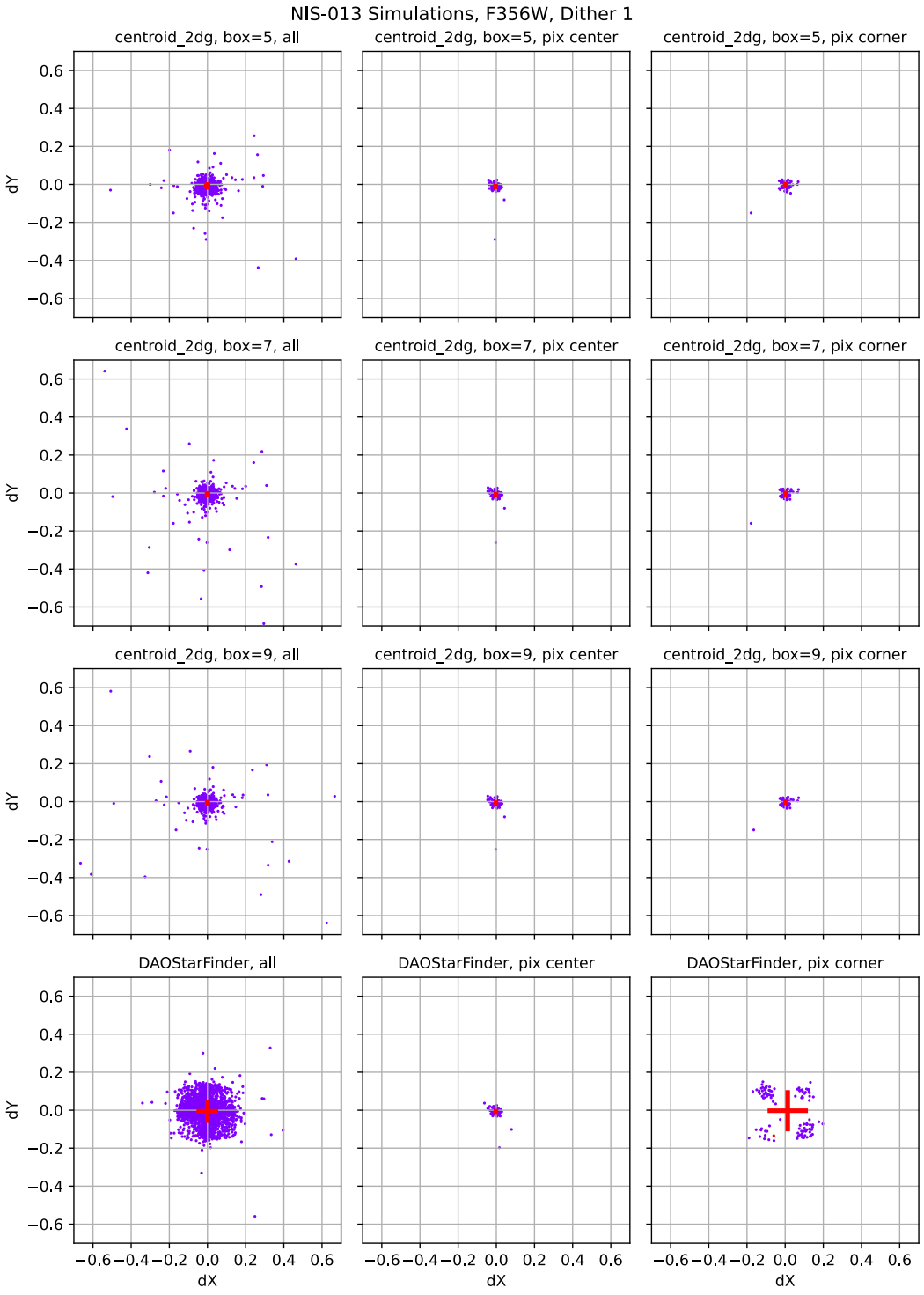

Figure 23: Same as Figure 2, but now for the F356W filter.

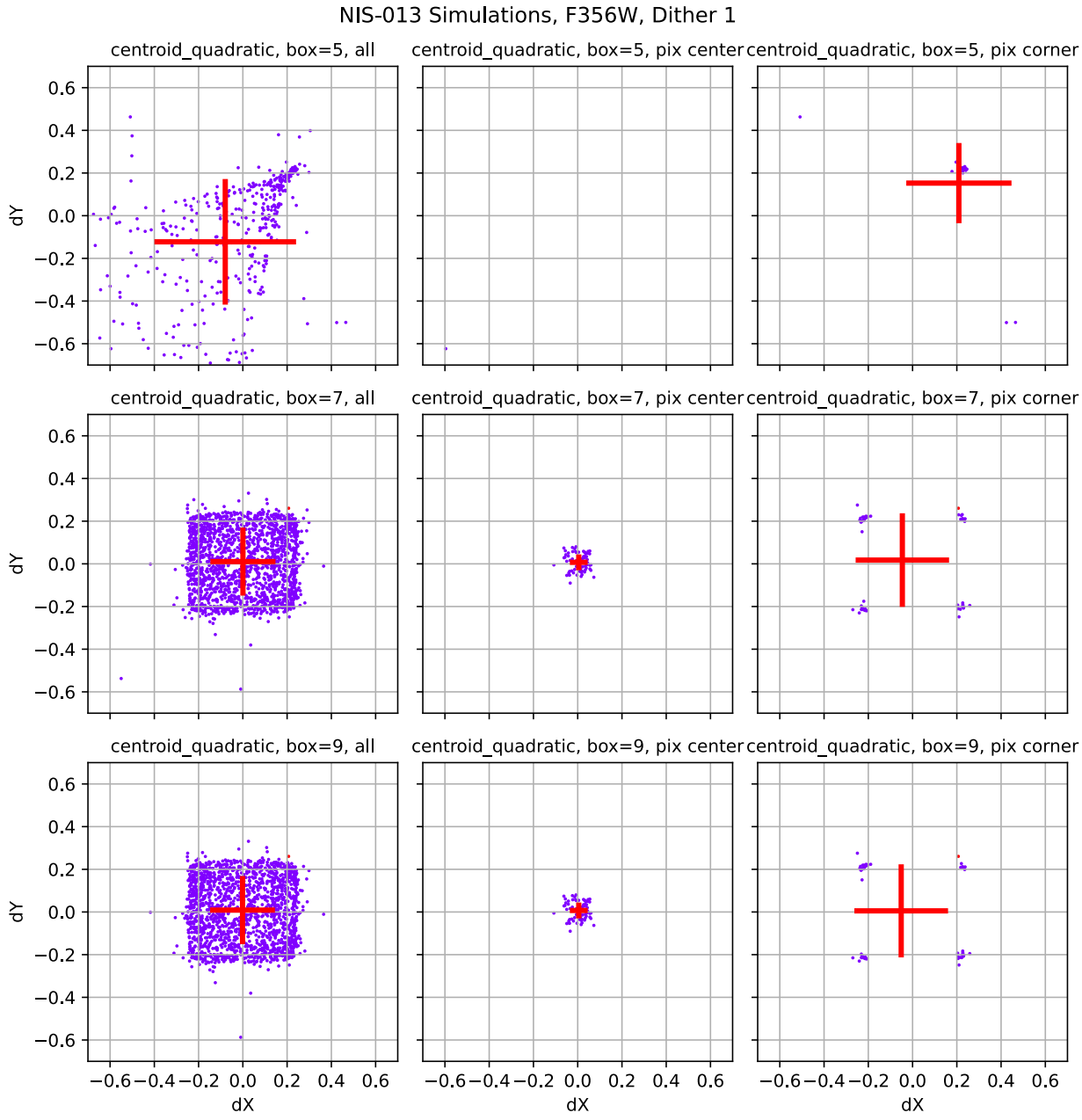

Figure 24: Same as Figure 3, but now for filter F356W.

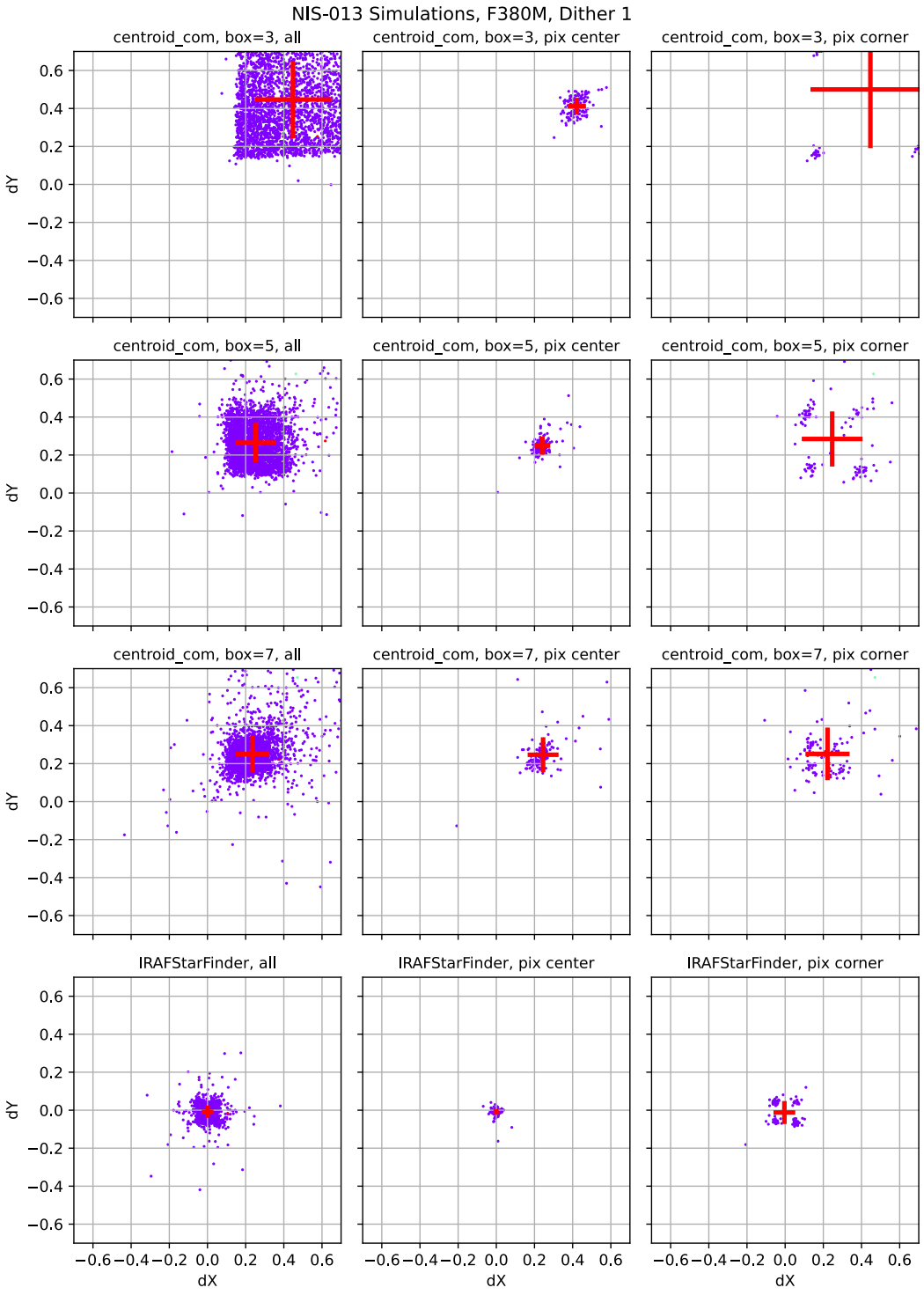

Figure 25: Same as Figure 1, but now for the F380M filter.

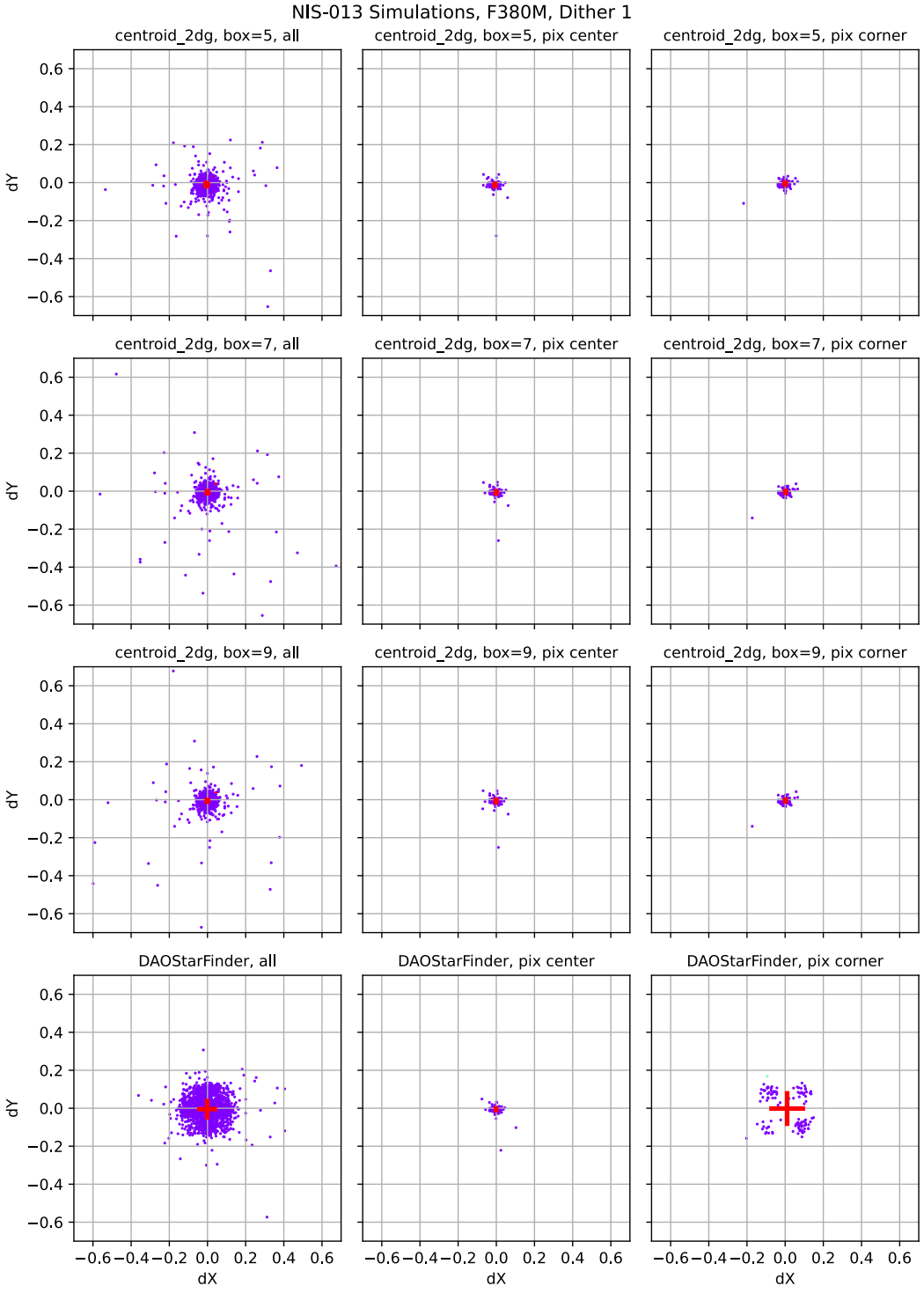

Figure 26: Same as Figure 2, but now for the F380M filter.

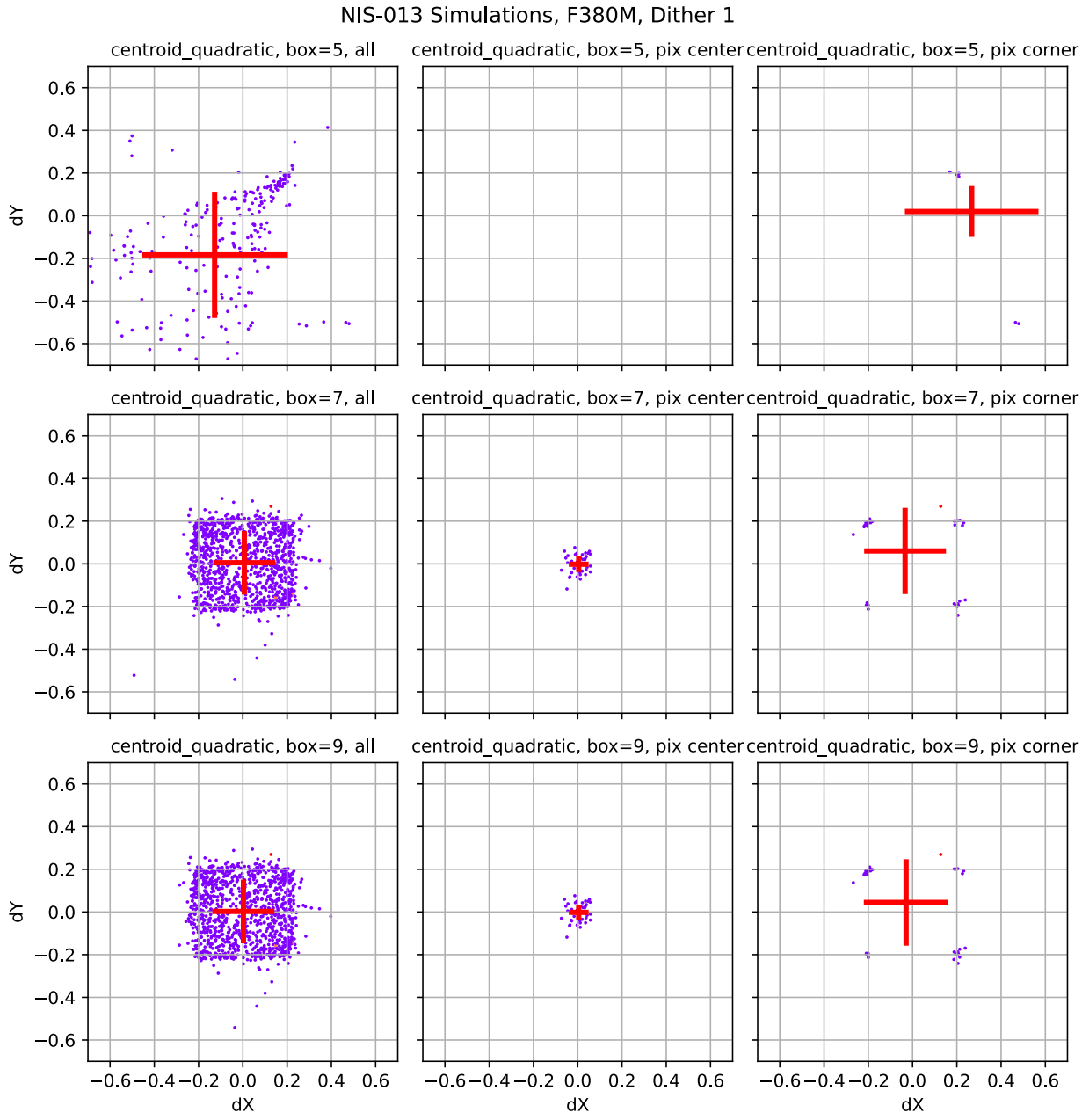

Figure 27: Same as Figure 3, but now for filter F380M.

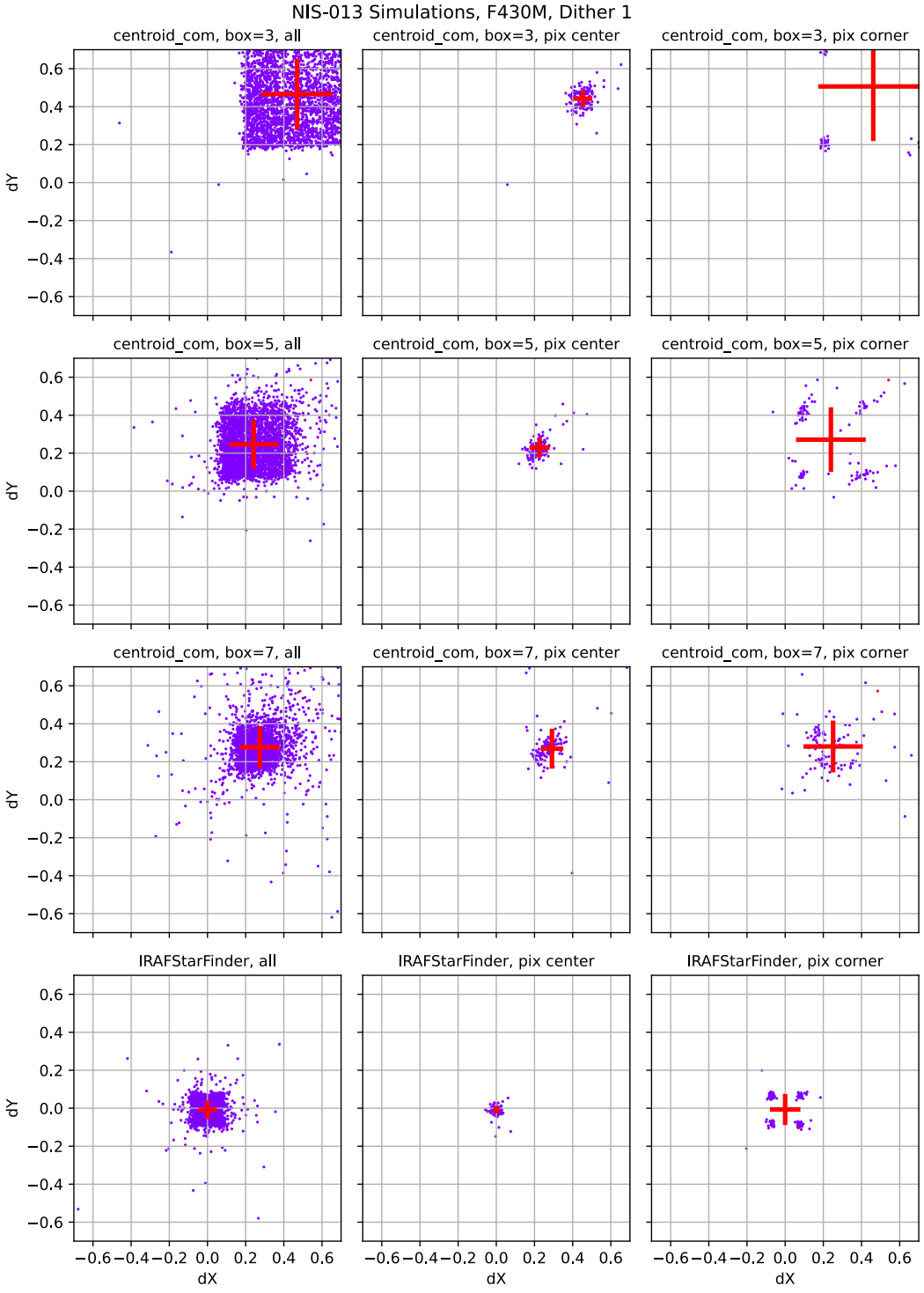

Figure 28: Same as Figure 1, but now for the F430M filter.

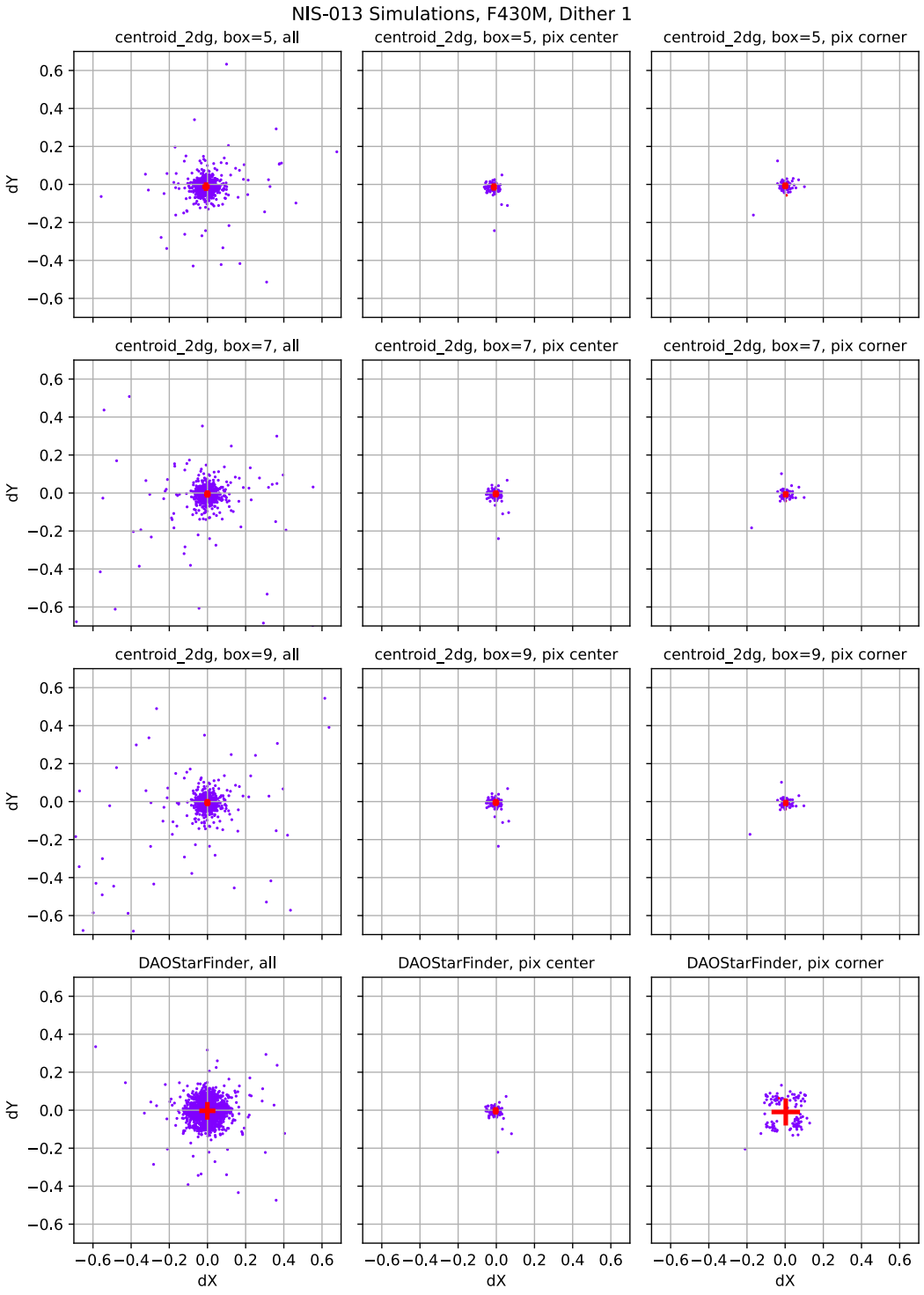

Figure 29: Same as Figure 2, but now for the F430M filter.

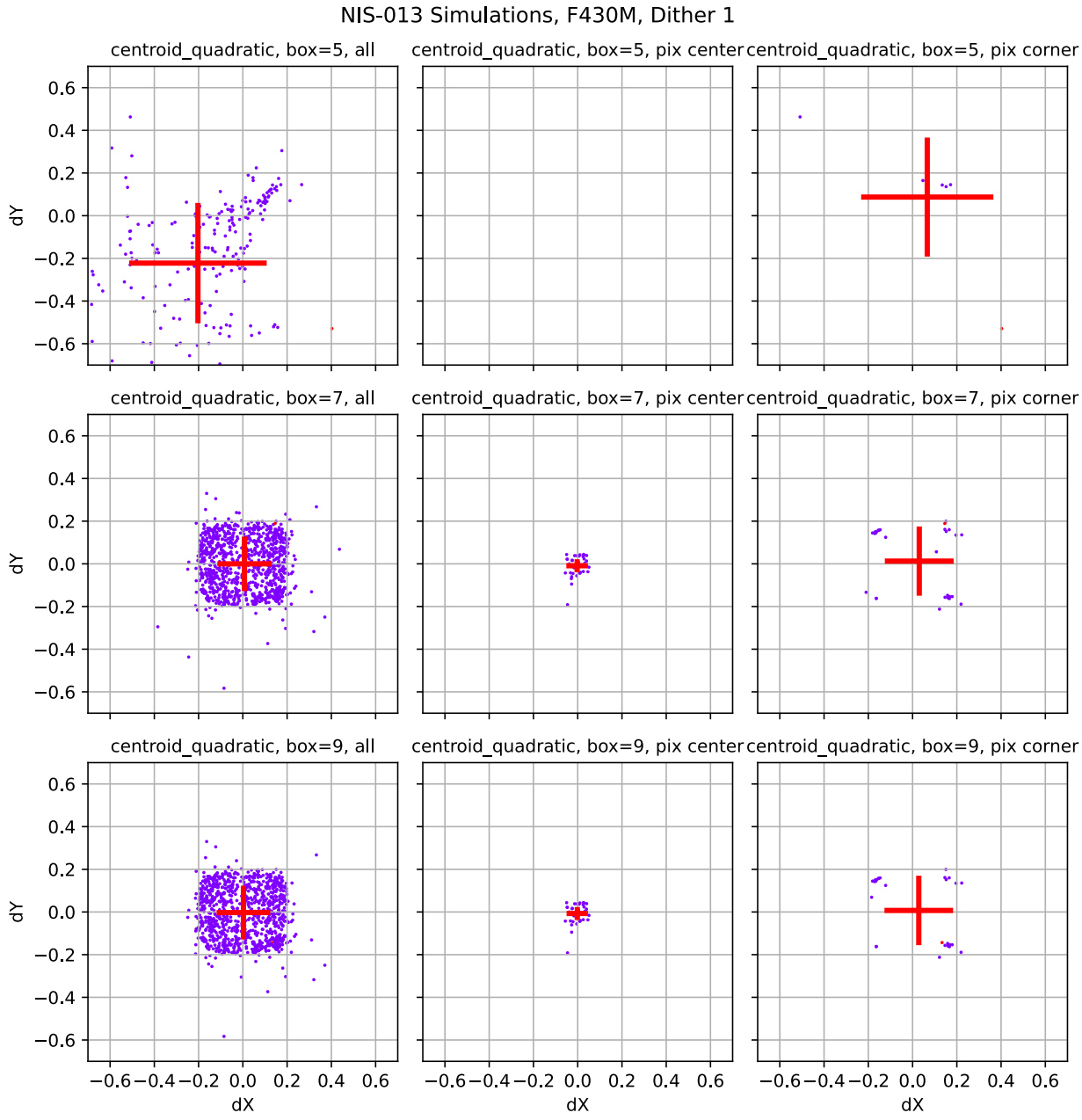

Figure 30: Same as Figure 3, but now for filter F430M.

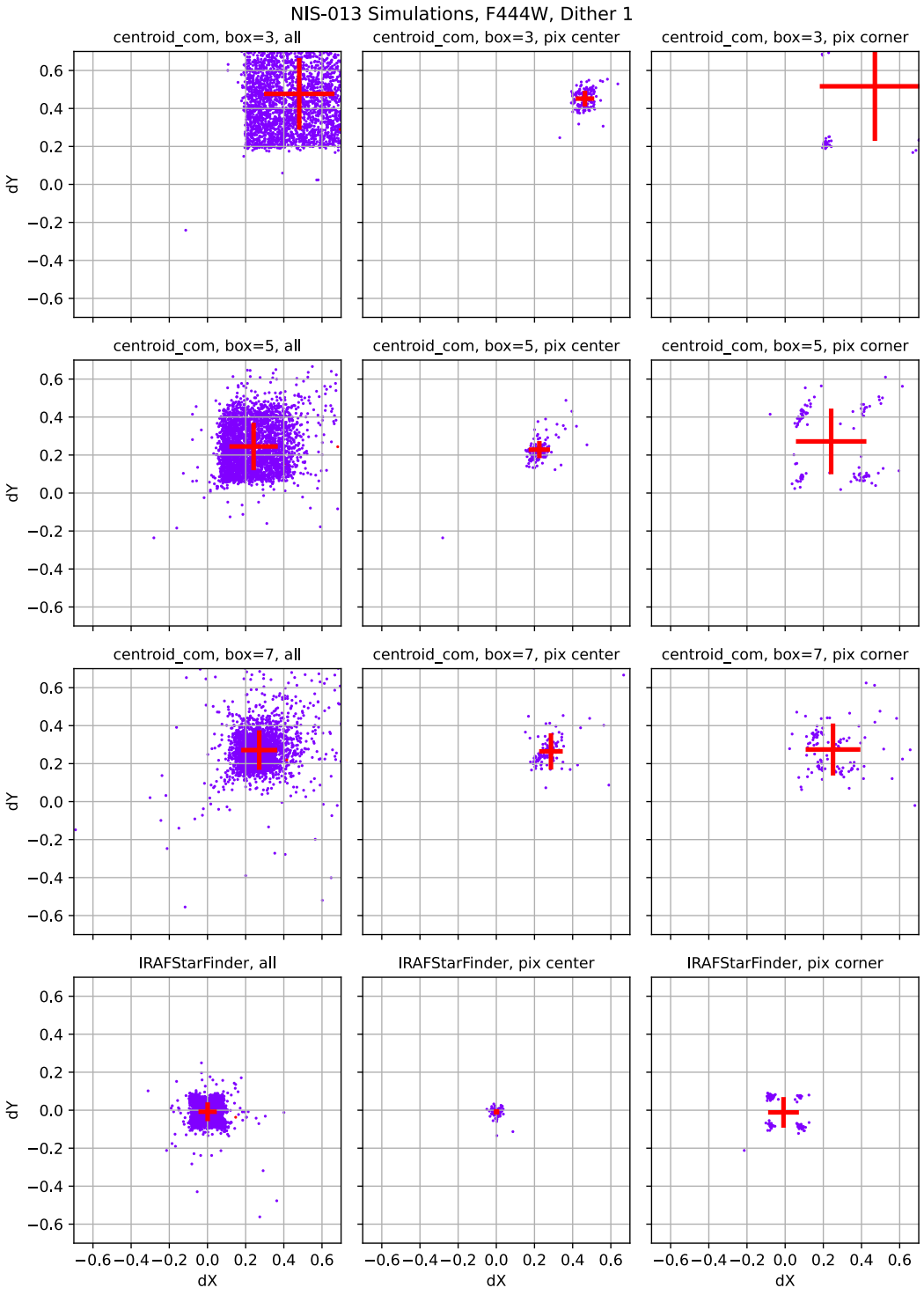

Figure 31: Same as Figure 1, but now for the F444W filter.

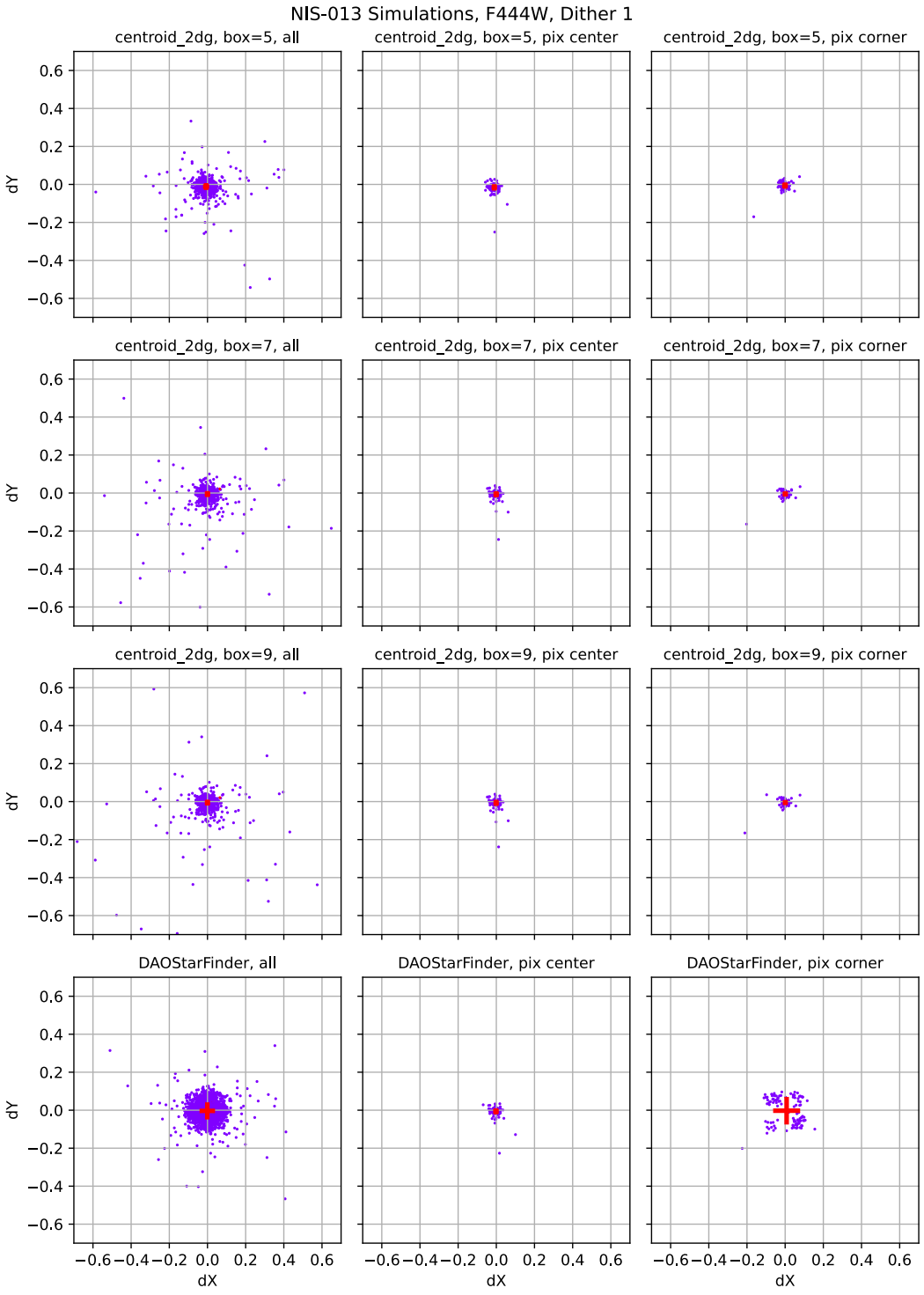

Figure 32: Same as Figure 2, but now for the F444W filter.

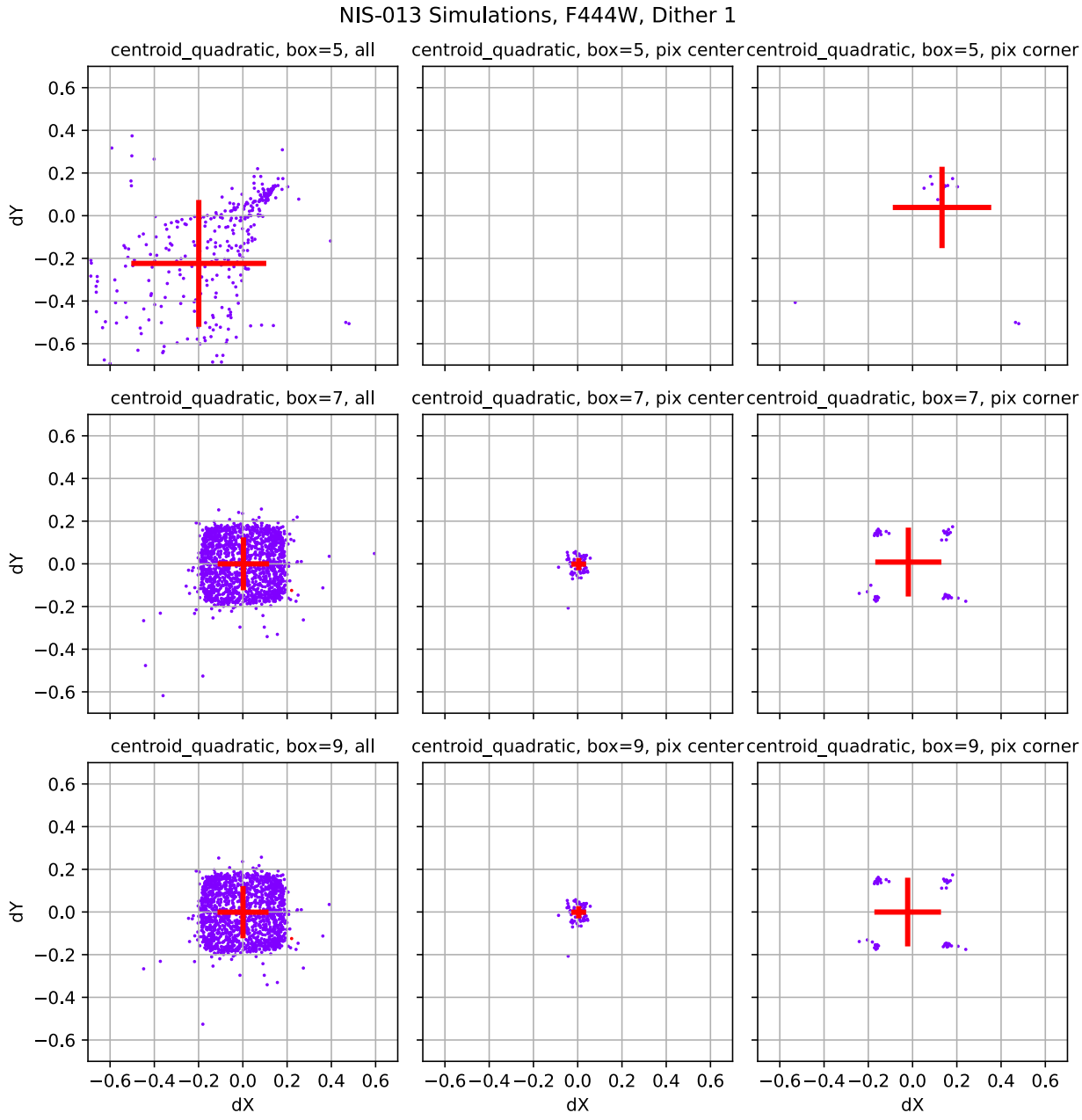

Figure 33: Same as Figure 3, but now for filter F444W.

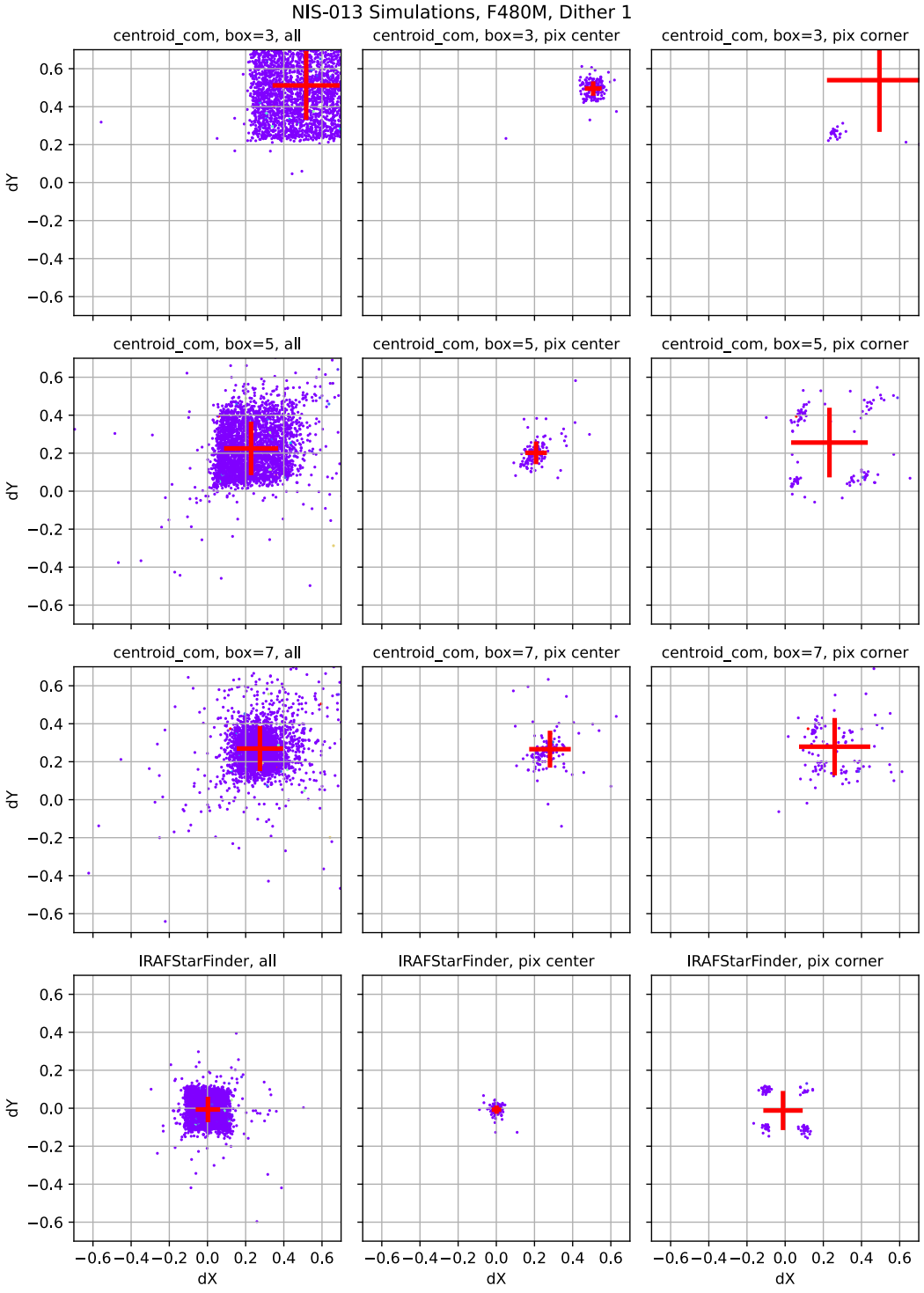

Figure 34: Same as Figure 1, but now for the F480M filter.

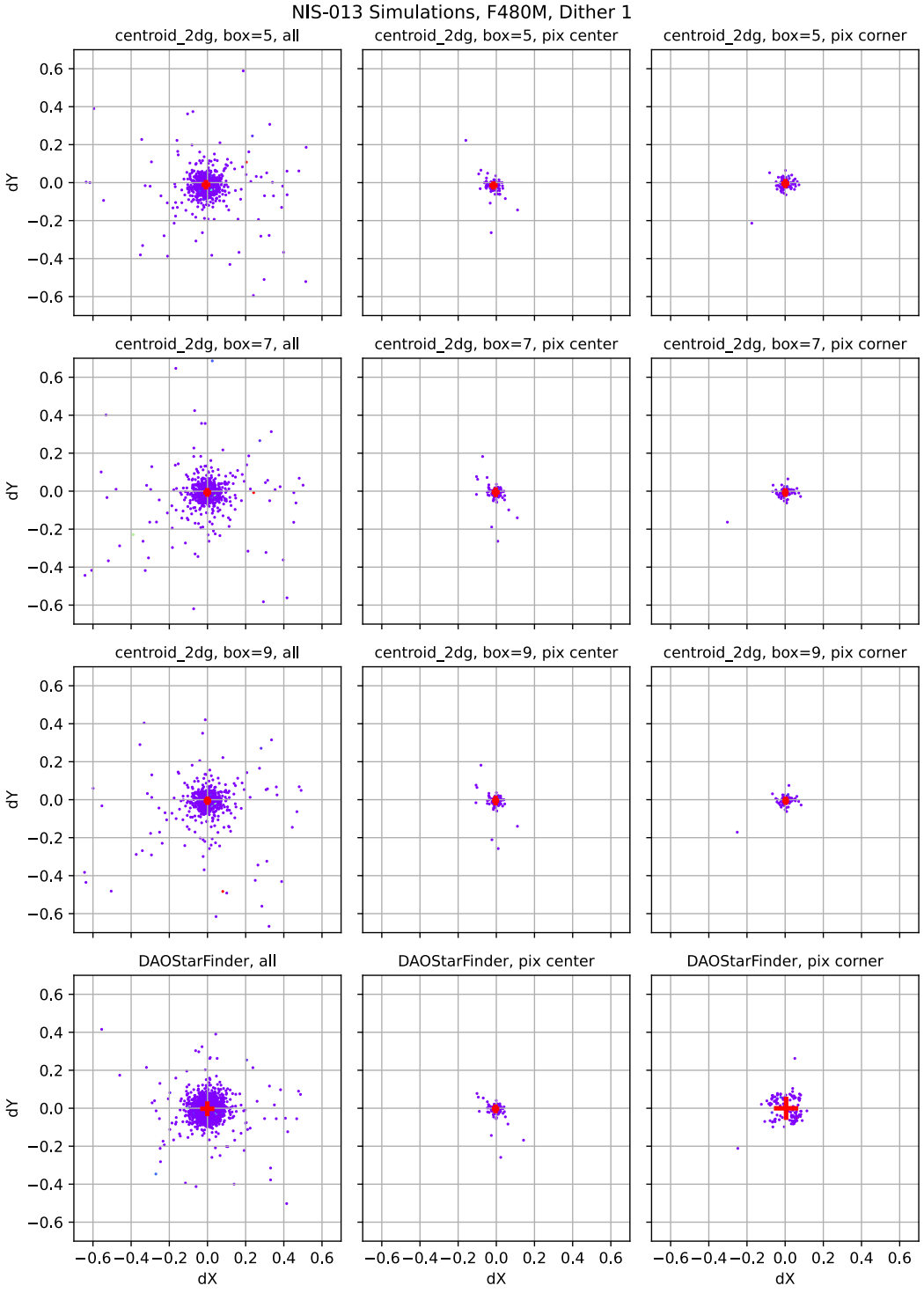

Figure 35: Same as Figure 2, but now for the F480M filter.

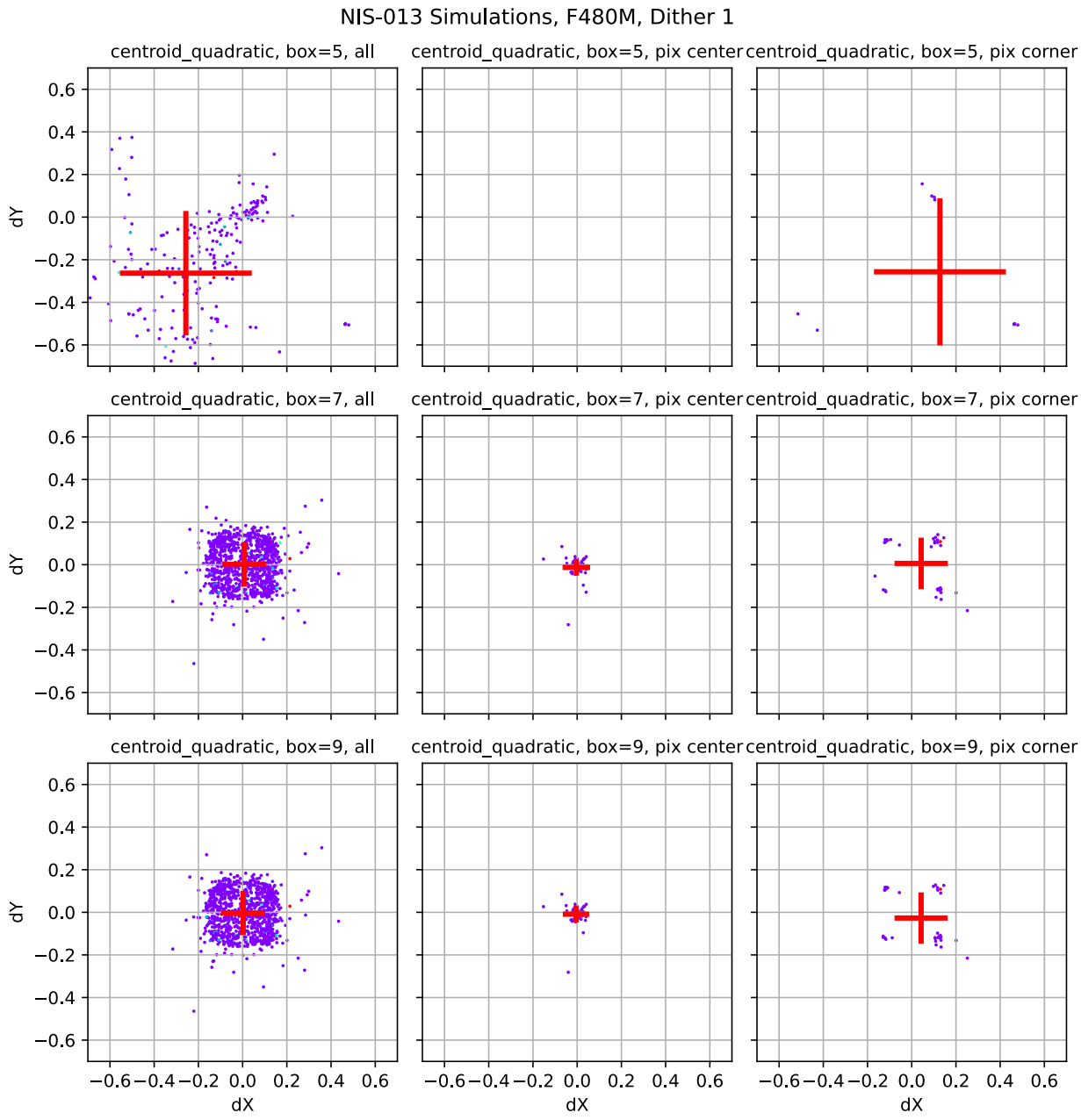

Figure 36: Same as Figure 3, but now for filter F480M.

6 Discussion and Trends

We discuss our findings below, starting with the results for the individual centroiding algorithms, followed by our general recommendations.

6.1 Center of Mass algorithm (centroid_func = centroid_com)

6.1.1 General Comments

This algorithm uses image moments to calculate the center of mass for each source in the input list. As can be seen in Figures 1-24, this method does not work very well with NIRISS PSFs. Centroids determined using this algorithm are found to be systematically off by of order 0.2-0.4 pixels, and the amplitude of this offset increases with increasing filter pivot wavelength (and thus PSF FWHM). Comparison of the results for "all stars" with those for stars positioned near pixel centers and stars near pixel corners reveals that the accuracy of this method is relatively sensitive to the placement of PSFs relative to pixel borders.

6.1.2 Dependence on Measurement Box Size

The sensitivity of this method on PSF placement relative to pixel borders is especially strong when used with relatively small measurement box sizes, for which the measured centroids for stars near pixel corners are found to cluster around distinct, clearly separated locations that are offset from the input position (see top right panels in Figures 1, 3, 5, …, 23). This feature persists for larger measurement box sizes as well, albeit at smaller offset amplitudes. Finally, Table 2 shows that the precision of this method decreases at box sizes > 5 pixels, especially for the NIS-011b field which is significantly more densely populated than the NIS-013 field.

6.2 IRAFStarFinder algorithm

Similar to the Center of Mass algorithm, `IRAFStarFinder` also uses image moments to calculate centroids. However, the main difference between the two methods is that `IRAFStarFinder` convolves the image with a circular Gaussian (with a user-provided FWHM) prior to the centroid measurement. As the results show, this smoothing step provides a significant improvement to the accuracy and precision of the resulting centroids. The dependence of the centroid precision on the placement of the PSFs relative to pixel borders and corners is still present for `IRAFStarFinder`, but it is less significant than for the `centroid_com` method.

6.3 2-D Gaussian algorithm (centroid_func = centroid_2dg)

6.3.1 General Comments

This method is found to yield the most accurate and precise centroids for NIRISS PSFs among the algorithms considered for this study. Systematic offsets from the input positions are in the range (0.000, 0.045), with the larger offsets being found for the filters with the shortest pivot wavelength and hence the most undersampled (or "intrinsically peaked") PSF. However, these offsets, as well as the standard deviations of the distribution of points around the mean offsets, are smaller than for all the other methods used here. Another trend with pivot wavelength is seen in the shape of the distribution of spatial offsets: this shape is square-like for the shorter pivot wavelengths and moves toward circular (i.e., more random) for longer pivot wavelengths, for which the PSFs become increasingly less undersampled. However, the Gaussian fits do not lead to a significant dependence of the centroid precision on the positioning of the PSF relative to pixel borders and corners, which constitutes an additional strength of this method.

6.3.2 Dependence on Measurement Box Size

The dependence of this method on measurement box size is small relative to that of the centroid_com method. Generally, the 5-pix box size works slightly better than the larger box sizes for the narrower PSFs (i.e., pivot wavelengths <~ 2 μm) whereas the 9-pix box size works slightly better for the filters with longer wavelengths. However, the differences are insignificant and any of the box sizes used here work well.

6.4 2-D Quadratic algorithm (centroid_func = centroid_quadratic)

6.4.1 General Comments

While this method yields very accurate *average* centroids for NIRISS PSFs (when averaged over thousands of stars across the field), it is very sensitive to placement of the PSF relative to pixel borders, as can be seen in Figures 3, 6, 9, …, 36. In fact, high-accuracy centers of individual PSFs are only achieved with this method for PSFs that are placed very close to pixel centers. This is due to the intrinsically relatively wide profile of quadratic functions, which do not provide accurate fits to narrow asymmetric distributions like undersampled PSFs. This is illustrated in Figure 37 below, which shows a 7-pixel 1-D profile of a NIRISS F090W PSF that was placed at X pixel 3.60 (i.e., 0.1 pixel away from a pixel boundary) and Y pixel 4.0 using `WebbPSF`. Overplotted are a best-fit Gaussian (in red) and best-fit quadratic functions with box sizes of 5 and 7 pixels (in blue and green, respectively). Note that the peaks of the quadratic functions (at X ~ 3.84) are effectively "pulled" toward the pixel with the highest value (i.e., X = 4) due to their wide profile relative to the PSF, while the Gaussian fit provides a much more accurate center (X = 3.63) due to its shape which provides a much better fit to the data. As such, we do not recommend the quadratic method for astrometry with NIRISS PSFs.

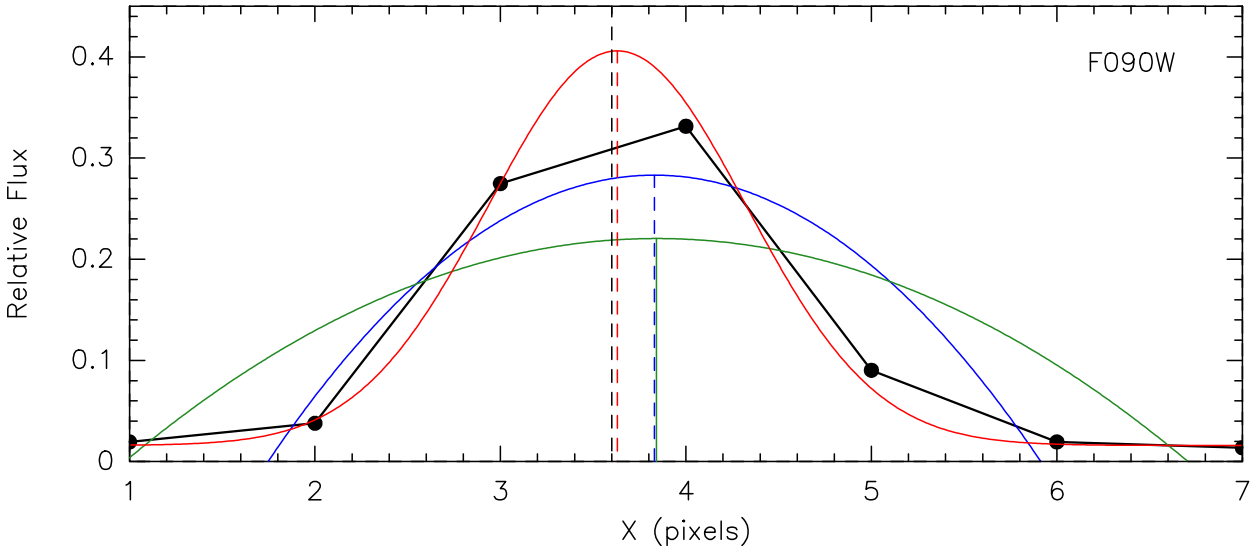

Figure 37: The black dots and lines represent a 1-D profile of a NIRISS F090W PSF centered on X = 3.60 (indicated by the vertical black dashed line). Overplotted are a best-fit Gaussian (in red), and the best-fit quadratic functions to the inner 5 and 7 pixels (in blue and green, respectively). Vertical dashed lines indicate the centroids of each function.

6.4.2 Dependence on Measurement Box Size

As is clear from a glance to the top panels in Figures 3, 6, 9, …, 36, the 2-D quadratic centroid algorithm regularly suffers from relatively large errors when applied to NIRISS PSFs with a measurement box size of 5 pixels, which is the default setting (!). The reason for this issue has not been investigated for this report. Other than that, differences between box sizes of 7 and 9 pixels are insignificant for all NIRISS filters.

6.5 DAOStarFinder algorithm

This method is found to be most susceptible to centroiding errors for undersampled PSFs. As illustrated by the bottom rows of panels in Figures 2, 5, 8, …, 35, spatial offsets due to centroid errors using this method on undersampled PSFs tend to be primarily distributed in a "plus pattern" centered near (dX, dY) = (0, 0), reaching significant offsets of larger than 0.7 pixel along each axis, along with a significant "cloud" with a relatively flat distribution in (dX, dY). It turns out that `DAOStarFinder` works very well for PSFs positioned close to pixel centers, but it often incurs significant centroid errors when an undersampled PSF is positioned near pixel corners, due to its use of 1-D Gaussian fits to projected light distributions. Note that the precision of `DAOStarFinder` improves significantly for Nyquist-sampled PSFs (e.g., filter F480M, see bottom panels in Figure 35), but we cannot recommend its use for NIRISS imaging given its poor performance for undersampled PSFs.

6.6 Further Insights from the Distribution of Spatial Offsets

Prompted by the finding of bimodal distributions of spatial offsets from the expected positions in X and Y during a recent rehearsal of the commissioning analysis plan (CAP) for NIS-011b (i.e., JWST program 1086) using the F150W filter in conjunction with the findings described above, we now consider the dependence of these distributions on the maximum distance from pixel centers in X and Y, which we refer to as R_{max} in the following. We describe and illustrate the results for one filter whose PSF is strongly undersampled (F150W) and for a filter whose PSF is Nyquist sampled (F480M). Furthermore, we compare only the two centroid algorithms that were found to perform well in general in the discussion above: `centroid_2dg` with box size = 9 pixels, and `IRAFStarFinder`.

Figure 25 shows the results for F150W, which we describe below in some detail.

- For the `IRAFStarFinder` method, if no restriction is applied to the star positions relative to pixel borders, the measured spatial offsets are found to cluster in four locations around the mean offset, separated from one another by ~6-7 mas in X and Y, corresponding to ~0.1 pixel. This is consistent with what was found during the CAP rehearsal mentioned above. When restricting the star positions by imposing $R_{max} = 0.2$, the distribution becomes significantly less bimodal; the bimodality disappears when imposing $R_{max} = 0.1$. While these restrictions on the star positions relative to pixel borders obviously cause significant reduction in the number of stars and hence increasing Poisson errors, these findings do explain the reason for the bimodality seen in the distribution of offsets for "all stars". Furthermore, the overall mean offsets (dX, dY) are found to stay independent of the value of R_{max} (to within the errors), suggesting that `IRAFStarFinder` is robust in terms of measuring mean offsets.

- For the `centroid_2dg` method, the bimodality of the distributions in dX and dY is much less prominent than for the `IRAFStarFinder` method when using "all stars". Note also that the mean offset in dY is closer to zero (and thus more accurate) for `centroid_2dg` than for `IRAFStarFinder`. For `centroid_2dg`, the distributions of dX and dY already become unimodal when imposing $R_{max} = 0.2$, and these distributions become more peaked when $R_{max} = 0.1$. Again, the mean offsets stay independent of the value of R_{max} to within the errors, lending credence to the robustness of this method when measuring mean offsets.

Results for filter F480M (whose PSF is Nyquist sampled) are shown in Figure 26. We mention a few things of note below in this regard:

- The 2-D distributions of offsets are much more uniform for filter F480M than for F150W, and the 1-D distributions of dX and dY are already unimodal for F480M when using "all stars". This is true for both `IRAFStarFinder` and `centroid_2dg`.
- For `IRAFStarFinder`, the distribution of offsets becomes significantly more peaked when decreasing R_{max}. However, the mean offsets again remain independent of R_{max} to within the uncertainties.
- The overall astrometric precision is significantly higher for `centroid_2dg` than for `IRAFStarFinder`. In fact, for `centroid_2dg`, the mean *as well as the standard deviation* of offsets is independent of the value of R_{max} for this filter, which really speaks to its strength in astrometry measurements relative to `IRAFStarFinder` and the other methods studied here.

7 Conclusions and Recommendations

- Given our findings described above, we recommend the use of the `centroid_2dg` algorithm with measurement box size in the range 5-9 pixels for measurements that demand the best possible astrometric precision, and where it is important that the dependence on PSF location within pixels be minimized. However, it should be realized that the `centroid_2dg` fitting algorithm incurs significantly longer run times than the other algorithms considered here. On a 16″ Macbook Pro with a 2.3 GHz 8-core Intel i9 processor and 32 GB internal memory, `centroid_2dg` took 203.5 s versus 0.7 s for `centroid_com`, for a list of ~7250 sources and a full-frame image of 2048 x 2048 pixels.
- Between the two source detection algorithms tested here (`DAOStarFinder` and `IRAFStarFinder`), we find that `IRAFStarFinder` is far superior for use with the (generally strongly undersampled) NIRISS PSFs. In fact, when used with carefully determined PSF FWHM values, its centroiding precision rivals that of the `centroid_2dg` algorithm in terms of measuring mean offsets; the main relative shortcoming of `IRAFStarFinder` is its stronger sensitivity to PSF placement within pixels. However, we expect that this shortcoming can be mitigated within image alignment applications such as `TweakReg` by allowing the user to iteratively discard outliers in a user-friendly way while converging to the final alignment solution. Alternative options on how to deal with this are (1) by letting `TweakReg` use only stars that are found to be within 0.2 pixel of pixel centers, and/or (2) by including a recentering step within `TweakReg` that uses the `centroid_2dg` algorithm.

Acknowledgments. We thank Tony Sohn, André Martel and Chris Willott for useful discussions, and Jay Anderson for a swift and thorough review of this report.

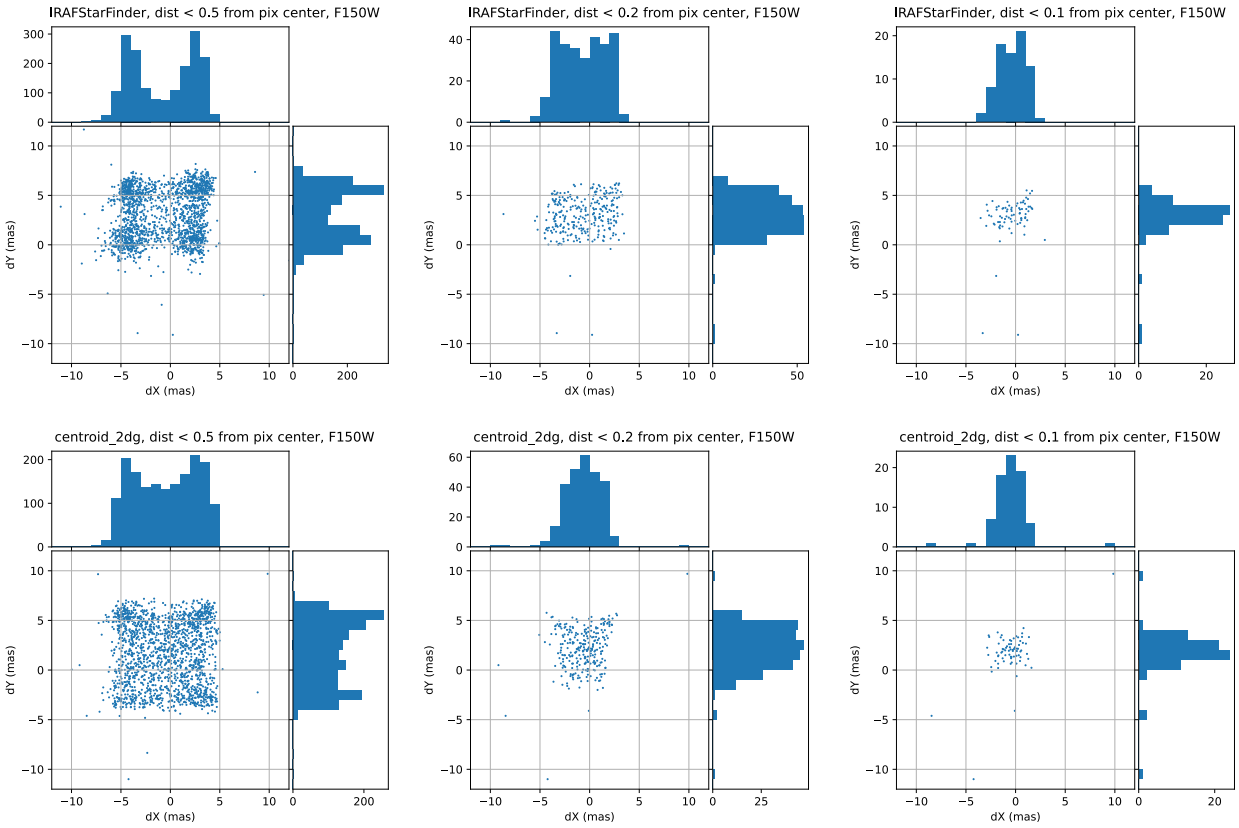

Figure 25: Distribution of spatial offsets in X and Y (in mas; note that 1 NIRISS pixel = 65.6 mas) for filter F150W as function of the maximum distance of the star location from pixel centers. The top row of panels is for the `IRAFStarFinder` method, while the bottom row is for the `centroid_2dg` method with box size of 9 pixels. The plot titles above the panels indicate the maximum distance of stars (in pixels, both in X and Y) from pixel centers (parameter R_{max} in the text). Note the significant dependence of the distributions of dX and dY on the maximum distance of stars from pixel centers for undersampled PSFs such as those for filter F150W.

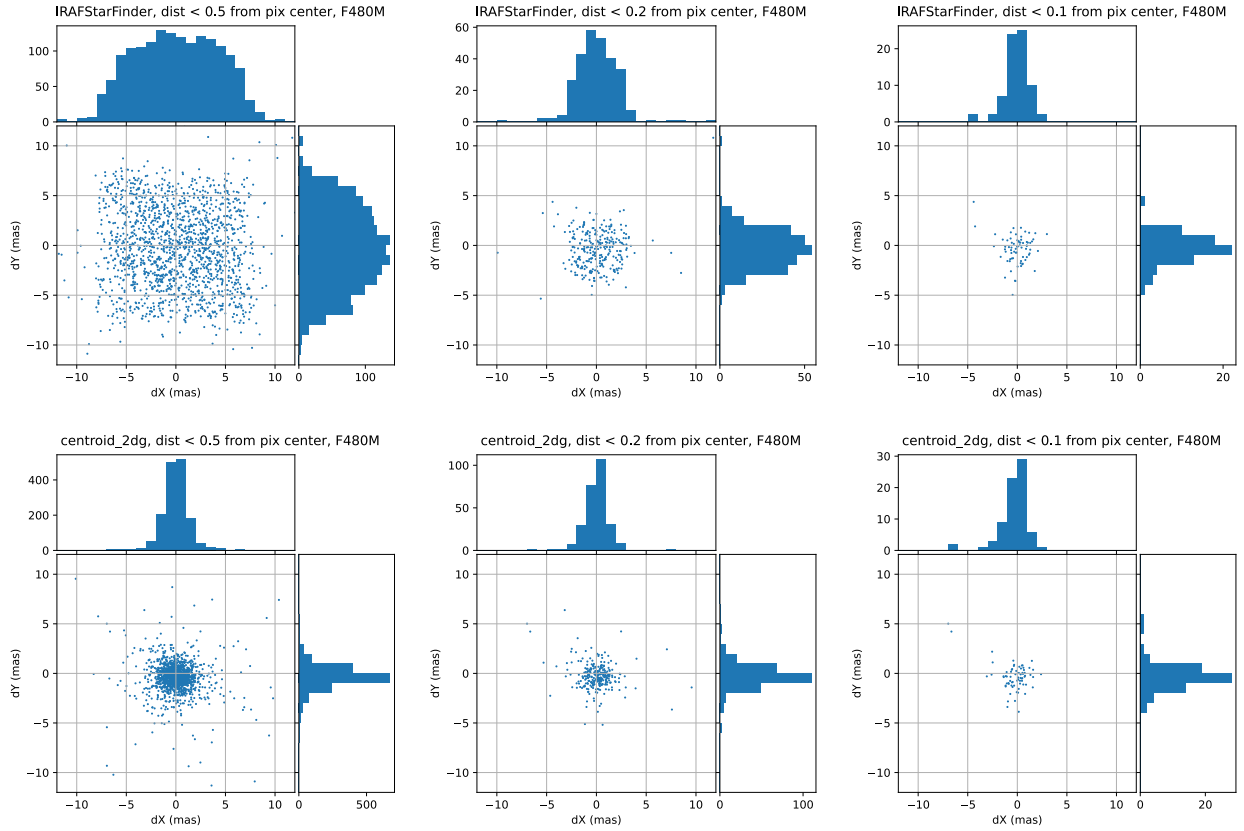

Figure 26: Same as Figure 25, but now for filter F480M. Note that dX and dY are much more uniformly distributed for F480M (whose PSF is Nyquist sampled) than for F150W (whose PSF is strongly undersampled) which was shown in Figure 25.

8 References

Anderson, J., & King, I. R., 2000, "Toward High-Precision Astrometry with WFPC2. I. Deriving an Accurate Point-Spread Function", PASP, 112, 1360

Astropy Collaboration, Robitaille, T. P., Tollerud, E. J., et al., 2013, "Astropy: A community Python package for astronomy", A&A, 558, A33

Astropy Collaboration, Price-Whelan, A. M., Sipõcz, B. M., et al., 2018, "The Astropy Project: Building an Open-science Project and Status of the v2.0 Core Package", AJ, 156. 123

Goudfrooij, P., et al., 2021, "NIRISS Operations Concept Document", CSA Technical Report CSA-JWST-CD-003, available through http://bit.ly/2BEq4et

Perrin, M., et al., 2012, "Simulating point spread functions for the James Webb Space Telescope with WebbPSF", Proc. SPIE 8842, 88423D

Perrin, M., et al., 2014, "Updated point spread function simulations for JWST and WebbPSF", Proc. SPIE 9143, 91433X

Sahlmann, J., 2017, "Astrometric Accuracy of the JWST calibration field catalog examined with

the first Gaia data release", JWST Technical Report JWST-STScI-005492

Sahlmann, J., 2019, "Astrometric catalog for JWST focal plane geometric calibration", JWST Technical Report JWST-STScI-006828

Stetson, P. B., 1987, "DAOPHOT: A Computer Program for Crowded-Field Stellar Photometry", PASP, 99, 191